

**NOVEL NONINVASIVE OPTICAL DIAGNOSTIC TECHNOLOGIES
FOR THE MANAGEMENT OF NEONATAL JAUNDICE**

A Dissertation
Submitted to
the Temple University Graduate
Board

In Partial Fulfillment
of the Requirements for the Degree
**DOCTOR OF PHILOSOPHY
BIOENGINEERING**

by
Brandon K. Harrison-Smith
Diploma Date June 2022

Examining Committee Members:

Dr. Chetan Patil, Advisory Chair, Bioengineering
Dr. Nancy Pleshko, Bioengineering
Dr. Mohammad Kiani, Bioengineering
Dr. Hendrik Weitkamp, TBD
Dr. Daniel Jacobs, External Reader, Mechanical Engineering

ABSTRACT

Optical Diagnostic (OD) approaches are used to assist in real-time disease screening and estimation of physiological parameters. OD techniques such as pulse oximeters, transcutaneous bilirubinometers (TcB) and infrared thermometers have become key components for point-of-care clinical management. TcB is used to screen infants for extreme or prolonged neonatal jaundice (hyperbilirubinemia), a treatable condition that can result in permanent neurological impairment or death. Poor outcomes are common in low- and middle-income countries (LMIC), but rare in high-income countries, where access to newborn TcB screening is one of several factors that contributes to disparities. A low-cost, widely distributable approach for TcB could help expand newborn screening in LMICs. Due to the rapid global adoption of versatile smartphones with onboard camera modules, there is increased interest in transforming mobile phones into OD devices, including for the purpose of performing estimates of circulating bilirubin levels in order to expand access to transcutaneous bilirubinometry (TcB) for neonatal jaundice screening.

In this dissertation, the feasibility of performing TcB using spatially resolved diffuse reflectance measurements acquired using a mobile phone is evaluated in human subject studies, as well as using theoretical modeling and optical phantom studies. In Aim 1 of this project, we report on the feasibility of a mobile phone-based TcB device and show the development of this device through Monte Carlo simulations. Theoretical models were constructed and utilized for predicting bilirubin levels and were then

evaluated with a small pilot study. We extracted measurements of reflectance from multiple optimized spatial-offset regions of interest (ROIs) and a linear model was developed and cross-validated. This resulted in a correlation between total serum bilirubin and mobile phone-based TcB estimated bilirubin values, with $R^2 = 0.42$ and Bland-Altman limits of agreement of +6.4 mg/dL to -7.0 mg/dL. These results report the feasibility of a mobile phone with a modified adapter that can be utilized to measure neonatal bilirubin values; thus creating a novel tool for neonatal jaundice screening in low-resource settings.

Aim 2 reports further evaluation of a multi-device mobile phone-based TcB study, including calibration for inter-device variability. Measurements of reflectance were extracted from multiple optimized spatial-offset regions of interest (ROIs) and a linear model was developed and cross-validated. This resulted in a correlation between total serum bilirubin and mobile phone-based TcB estimated bilirubin values, with $R^2 = 0.28$ and Bland-Altman limits of agreement of +9.2 mg/dL to -9.3 mg/dL. These results indicate that an adapter-based smartphone can be modified to measure neonatal bilirubin values for neonatal jaundice screening in low-resource settings.

Finally, Aim 3 seeks to guide future developments and evaluate theoretical performance of spatially resolved diffuse reflectance image measurements for regression-based estimation of optical chromophores. We perform a phantom study to explore the impact that increased sample chromophore dimensional variability has on the predictive model correlation. Phantoms were created to simulate the variability of blood, bilirubin and melanin, and then images were captured with mobile phone-based TcB devices. Mean

intensities of systematic selection regions of interest based on spatial and spectral images were used as predictive variables for multiple linear regression model construction. The results of this study suggest that 2d spatially resolved diffuse reflectance models benefit the most from unique spatial and spectral regions of interests.

TABLE OF CONTENTS

	Page
ABSTRACT.....	ii
LIST OF FIGURES	viii
CHAPTER	
1. INTRODUCTION	1
2. BACKGROUND	4
Light-Matter Interactions	4
Biophotonics Overview	7
Diffuse Reflectance Overview	8
Overview of Skin Structure, Composition and Optical Properties	12
Neonatal Jaundice	13
Management of NNJ	15
Clinical Transcutaneous Bilirubinometry	17
3. DEVELOPMENT OF A MOBILE PHONE CAMERA BASED TRANSCUTANEOUS BILIRUBINOMETER FOR LOW-RESOURCE SETTINGS.....	21
Abstract.....	21
Introduction.....	22
Materials & Methods	24
Monte-Carlo Modeling of a Smartphone Based TcB Device	24
Mobile Phone TcB Optical Adapter	27
Diffuse Reflectance Measurements and Calibration.....	28

Human Subjects	29
Image Pre-Processing.....	31
Development of Region of Interest (ROI) Based Generalized Linear Model	31
Results.....	36
Monte Carlo Model.....	36
Mobile Phone TcB Design and Characterization.....	37
Pilot Study Results	37
Discussion.....	39
Conclusion	43
4. FEASIBILITY STUDY OF MOBILE PHONE-BASED TCB APPROACH TO IMPROVING THE MANAGEMENT OF NEONATAL JAUNDICE.....	44
Abstract.....	44
Introduction.....	44
Materials & Methods	47
Human Subjects	47
Device Measurements	48
Region of Interest (ROI) Based Generalized Linear Model	50
Multi-Site Calibration Method.....	51
Results.....	53
Discussion.....	53
5. IN SILICO ANALYSIS OF BILIRUBIN QUANTIFICATION USING SPATIALLY RESOLVED DIFFUSE REFLECTANCE WITH A MOBILE PHONE CAMERA	56
Abstract.....	56

Introduction.....	57
Materials & Methods	60
Tissue Optical Phantoms.....	60
Mobile Phone TcB Measurements.....	64
Regression Model Construction.....	64
Results.....	65
Discussion.....	74
Conclusion	77
6. PERSPECTIVE AND CONCLUSION	78
Mobile Phone-Based TcB	80
Future Direction	82
7. OUTPUTS AND DELIVERABLES	86
BIBLIOGRAPHY.....	88

LIST OF FIGURES

	Page
Figure 2-1. The Electromagnetic Spectrum [2].	5
Figure 2-2. Light Matter Interactions.....	6
Figure 2-3. Tissue Diffuse Reflectance.	9
Figure 2-4. Skin Layers [38].....	13
Figure 2-5. Jaundice in Neonates [40], [41].	14
Figure 2-6. Global Impact of NNJ [40], [41].....	16
Figure 2-7. Icterometry in Neonates [40], [41].....	16
Figure 2-8. Transcutaneous Bilirubinometers [40], [41].	17
Figure 2-9. Mobile Phone-Based Bilirubin Devices [51]–[53].	20
Figure 3-1. (A) 3D physical model of the mobile phone TcB design which depicts illumination through the device. An MC photon fluence map depicts modeled light distribution in neonatal skin. (B-C) Monte Carlo simulation results: (B) Normalized reflectance for two configurations and (C) Percent increase of reflectance from 0mm to 1.6mm configurations in the red, green and blue filtered channels.	25
Figure 3-2. Implemented Smartphone-Based TcB Device: (A) 3D printed adapter which guides light towards skin and house the band-pass filters. (B) Device attached to the phone casing with filters. (C) Smartphone application interface while taking a measurement from skin.	28
Figure 3-3. Human Subject Study: (A) Number of neonates used in the study. (B) Serum bilirubin distributions of neonates where majority of TSB values are clustered around 5-10 mg/dL.....	30
Figure 3-4. Two-Stage ROI-based GLM. Images and ROI initial positions for (A) Red (2 ROIs), (B) Green (3 ROIs) and (C) Blue (4 ROIs) channels. (D) The overview of the two-stage ROI optimization and model cross-validation algorithm. Input, intermediate and output data depicted as orange boxes; primary operations as purple boxes and secondary operations as green boxes.	32

Figure 3-5. Images with final ROI positions for (A) Red (2 ROIs), (B) Green (3 ROIs) and (C) Blue (4 ROIs) channels generated after stage 1 ROI optimization.....	36
Figure 3-6. Linear regression statistics (A) Correlation and (B) Bland-Altman of the mobile phones predicted bilirubin values vs. TSB values (n=37 patients).....	38
Figure 4-1. Study Demographics. (A) Racial Ethnicity of patients enrolled in the study: 61 Africans, 7 African Americans, 15 white and 8 race unknown neonates. (B) Enrolled neonates corresponding serum bilirubin values.	48
Figure 4-2. Mobile Phone TcB Device	49
Figure 4-3. Calibration Method for Aggregation of the Data.	52
Figure 4-4. Linear Regression Statistics. (A) ROI position. (B) Correlation of Device predictive [Bi] vs TSB [Bi] n=91. (C) Bland Altman of Device Bias and Confidence.	52
Figure 5-1. Phantom Fabrication and Image Analysis. (A) Fabrication of two layer skin mimicking PDMS optical phantoms. (B) Imaging of phantoms with the mobile phone-based TcB device (a modeled representation of the device and setup. Not to scale). (C) Single channel representative image from a phantom. (D) Image analysis and regression model construction procedure.	61
Figure 5-2. Phantom Chromophore Variability Matrix. (A) Depicts the compositional makeup of optical phantoms where each slice represents different melanin concentrations. (B) Representative picture of the phantoms where superficial melanin layer is shown with dashed border.	63
Figure 5-3. Region of Interest (ROI) Positioning. (A) Placement of a single ROI represented by a yellow arc. (B) The placement of two ROIs represented by a yellow arc and a cyan arc. (C) The placement of three ROIs represented by a yellow, green and cyan arc.	65
Figure 5-4. Simple univariate regression model for yellow dye 6 with 1 blue channel ROI where concentration of coffee and red dye was fixed. (A) Regression models for 3 unique red dye concentrations and low coffee concentration based phantoms concentration used for model construction. (B) Regression models for 3 sets of varied high coffee concentration based phantoms used for model construction. (C) R^2 and P values for the linear regression models created in Figure 5-4A-B. Here, cyan represents the phantoms with the lowest concentration of yellow dye 6, magenta for the middle concentration of yellow dye 6 and black for the highest concentration of yellow dye 6.....	67

Figure 5-5. A simple univariate regression model for yellow dye 6 varies with ROI placement position. Linear regression models were constructed with 1 blue channel ROI with a fixed concentration of coffee and red dye. (A) Arc position placement. Arc was translated from position-1 to position-15 in uniform increments. (B) Models were created from 15 different Arc positions. The darkest shade of black represents the position-1 regression line, lightest shade represents position-15. The red arrows show the movement of the regression line from the initial position to the final position. (C) P-values for each linear regression model created in Figure 5-5B. (D) R^2 values for each linear regression model created in Figure 5-5B. 68

Figure 5-6. Linear regression for yellow dye 6 with varying red dye and fixed coffee concentration with less than two ROIs (A) 1 blue channel ROI; (B) 2 blue channel ROIs; and (C) 1 blue and 1 green channel ROI. (D) P-values and R^2 values for each linear regression model created in Figure 5-6A-B. Red indicates the phantoms with lower coffee concentrations and green indicates the phantoms with higher coffee concentrations. 70

Figure 5-7. Linear regression models for yellow dye 6 with varying concentration of red dye and coffee with two to six ROIs. (A) 1 blue and 1 green channel ROI; (B) 1 blue, 1 green and 1 red channel ROI; and (C) 2 blue, 2 green and 2 red channel ROIs. (D) P and R^2 values for each linear regression model created in Figure 5-7A-C. Orange indicates the regression line created from all phantoms. 71

Figure 5-8. Linear regression models for yellow dye 6 with varying concentration of red dye and coffee with six ROIs. (A) 2 blue, 2 green and 2 red channel ROIs; (B) 3 blue, 2 green and 1 red channel ROIs; and (C) 2 blue, 3 green and 1 red channel ROIs. (D-F) represent models respective to Figure 5-8A-C, but with arc placements moved away by 100 pixels from the source. (F) P and R^2 values for each linear regression model created in Figure 5-8A-F. 73

1. INTRODUCTION

Optical Diagnostic (OD) approaches are used to assist in screening or identifying the presence of a disease. OD techniques such as pulse oximeters, transcutaneous bilirubinometers, infrared thermometers and many other devices have become key components for the management of many diseases. The greatest advantage of OD approaches is their ability to quantify physiological properties of the skin instantaneously. Physicians can then provide early and proper treatment to the patient based on this gathered information.

The development of OD approaches is directly tied to the evolution of biophotonic technologies, leading to an increase in development of novel noninvasive techniques. Emerging technologies such as Spatial Frequency Domain Imaging or Hyperspectral Imaging has been successful at expanding diagnostic capabilities to the evaluation of tissue across a 2d spatial and spectral platform. Due to the expanding accessibility of mobile phones, there is building interest in transforming mobile phones into optical diagnostic devices. The power of the mobile phone is in its versatility for taking images, running multiple applications, information transfer and its commonplace use in everyday life. There are many different OD applications that utilize the mobile phone's camera and flash. Multiple groups have started to explore the use of the mobile phone to take bilirubin measurements in order to increase accessibility of transcutaneous bilirubinometry screening techniques for neonates diagnosed with jaundice.

Neonatal Jaundice is a commonly occurring condition in neonates; and extreme or prolonged neonatal jaundice (hyperbilirubinemia) can result in permanent neurological impairment or death. Such outcomes are rare in high-income countries, but common in sub-Saharan Africa and low- and middle-income countries (LMIC). Effective treatment of neonatal jaundice is possible with phototherapy; however, screening requires accurate quantification of serum bilirubin levels, which can be challenging in LMICs. In the United States, transcutaneous bilirubinometry (TcB), a noninvasive technique based on optical diffuse reflectance, offers objective screening of infants for hyperbilirubinemia prior to hospital discharge. Studies have reported potential benefits of TcB adoption in LMIC; however, limitations include the high cost of TcB devices and reduced accuracy in infants with darkly pigmented skin.

When discussing OD techniques such as TcB, it is important to have an understanding of the basic principles of light and light-matter interactions. The background section will describe light interaction with biological tissue, followed by a survey of the field of biophotonics, in which optical techniques are developed for biological research, diagnosis, therapy, monitoring, imaging and surgery. Next, we will explore the optical technique diffuse reflectance spectroscopy and linear regression models for a basic overview of the field of transcutaneous measurements.

Transcutaneous measurement configurations are common in many diagnostic approaches, including TcB, and are also heavily impacted by the optical properties of the skin. Therefore, we will also further review the properties and compositions of the skin. Finally, the background will conclude with a review neonatal jaundice, management,

clinical TcB and modern TcB approaches. The topics discussed in this background will provide a foundational understanding of transcutaneous approaches for neonatal jaundice and guide the theoretical basis for future mobile phone-based transcutaneous measurements.

The focus of this dissertation is to show the feasibility and theoretical modeling framework of using a mobile phone as a TcB device to predict bilirubin levels. In Aim 1 of this project, we report on the feasibility of a mobile phone-based TcB device and show the development of this device through Monte Carlo simulations. Theoretical models were constructed and utilized for predicting bilirubin levels and were then evaluated with a small pilot study. Aim 2 reports further evaluation of the mobile phone-based TcB device through a multi-device and site study. Multiple mobile phone-based TcB devices were calibrated in order to bring data together for a larger study evaluation. Aim 3 seeks to evaluate the impact of spatial and spectral measurements of 2d spatially resolved diffuse reflectance model construction. Finally, future works, innovation, novelty of the Aims and a final conclusion are reported in this body of work.

2. BACKGROUND

Light-Matter Interactions

Light is traditionally described as both a wave and a particle, which can be expressed as electromagnetic radiation [1]. The electromagnetic spectrum demonstrates a range of frequencies of electromagnetic radiation with their corresponding wavelengths and energies. Radiation in this spectrum is characterized by frequency bands with different wavelengths as shown in Figure 2-1. Low frequency is associated with long wavelengths and high frequency is associated with short wavelengths. There are two main relationships derived from wavelength and frequency; these equations are the speed of light and the Planck Equation. The speed of light equation states that the speed of light (C) is directly proportional to relative wavelength and frequency. The Planck equation states that the measure of energy (E) is directly proportional to Planck's constant (h) and its frequency. These two equations are important for relating energy to wavelengths. Short wavelengths carry high energy and long wavelengths carry low energy.

$$C = \lambda\nu$$

$$E = h\nu$$

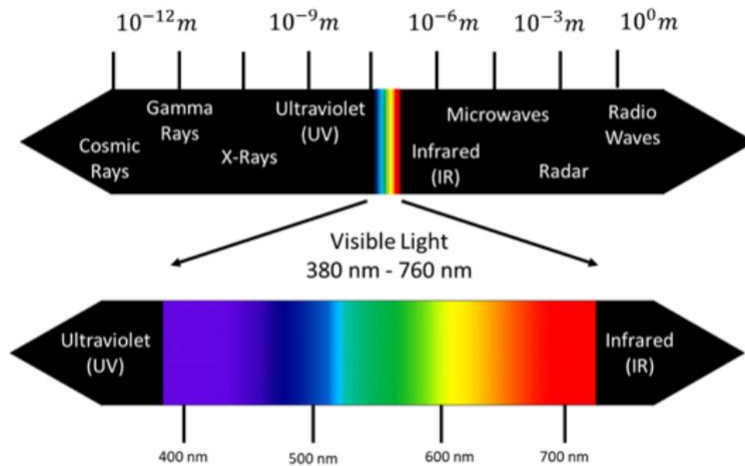


Figure 2-1. The Electromagnetic Spectrum [2].

When light interacts with matter, it is said to be delivering a photon packet of energy to the substance. The frequency, wavelength, speed and energy of the photons allow for unique interactions with the molecules inside matter. These interactions can range from reflection, absorbance, scattering and transmittance, which are depicted in Figure 2-2. Surface reflection can be observed as being specular or diffuse. Specular reflection occurs when the incident light strikes the surface and then reflects off of the surface at an angle equal to the incident light's angle. Diffuse surface reflectance happens when the surface is rough, causing the angle to reflect very differently to the incident angle. Transmittance occurs when light travels through a material. These interactions help produce unique optical properties which can be measured in terms of absorbance and scattering.

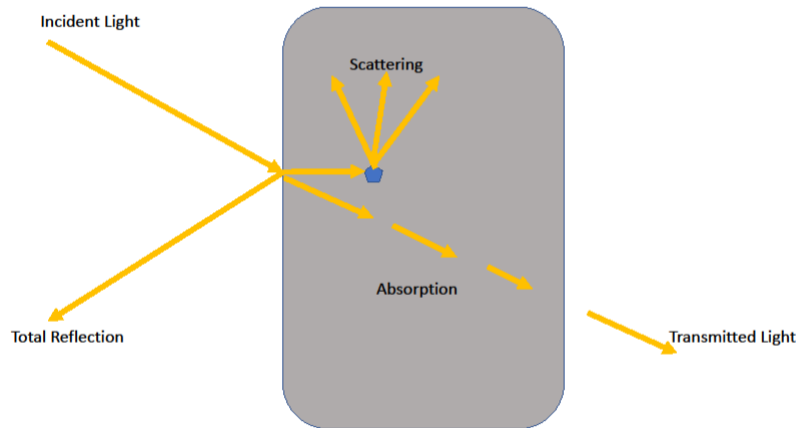


Figure 2-2. Light Matter Interactions.

Light scattering in collision with matter can take on two forms known as Mie and Rayleigh scattering. Mie scattering occurs when an elastic scattering of light interacts with particles that have a diameter similar or larger than the incident wavelength. Rayleigh scattering, on the other hand, occurs when an elastic scattering of light interacts with particles that are much smaller than the incident wavelength. Through absorption, light has the ability to transfer energy to the particle and transform it into vibrational energy. Analytical equations, such as the Beer-Lambert law, are used to relate the absorption of light through a material to the concentration of the material [3]. These analytical equations can then be used to develop approaches that calculate concentration from light-matter interaction. Light-matter interaction has been shown to be unique to the quantity and quality of the material in which the light interacts with, and these principles translate

directly to light's interaction with biological tissues and serve as the underlying physical principles that inform the development of many optical diagnostic techniques.

Biophotonics Overview

Biophotonics is a scientific field at the intersection of life and light sciences. This field has become instrumental in the development of life science research, therapy, monitoring, imaging, diagnostics and surgery [4]. Technological advancements, along with the discovery of new materials, has led to the structural advancement of many healthcare practices. Light that can penetrate the skin offers potential therapeutic uses or diagnostic analysis. Unique uses of lasers and optics have brought about a multitude of approaches that have been developed to create new forms of treatment and diagnostics, which in turn has improved patient outcomes and treatment options.

Lasers have been known to be utilized for a variety of therapeutic practices. In these approaches, the radiation is emitted in a controlled manner to address a medical issue [5]. For example, laser refractive surgery is a common therapeutic practice where lasers correct visual defects such as nearsightedness, astigmatism and farsightedness [6]. In this process, lasers are used to ablate tissue from the cornea to produce changes in the refractive power of the eye. Optical therapeutics can also be observed in photodynamic therapy, a photochemical approach that selectively destroys tissues. This technique is more commonly used for cancer therapy and treatment.

Exploration of tissue diagnosis is an additional application of lasers. One of the main advantages of this technique is the ability to provide quantitative measurement of

physiological differences or tissue classification [7]. This is typically accomplished with spectroscopic or imaging approaches that take advantage of light-tissue interactions, such as absorption and scattering [8]. A common spectroscopic example of this can be seen in pulse oximeters that measure blood oxygen levels. Here, single spectral channels are used in conjunction with analytical models to create predictions of blood oxygen levels [3]. Spectroscopic techniques can also be used in conjunction with fiber optic probes to take measurements of organs, such as the lungs, colon or bladder.

Lasers and optics further impact the healthcare field through the use of imaging. X-ray mammography is a commonly used screening technique for many cancers or bone fractures [9]. However, this technique heavily irradiates the patient and can be inconclusive at times. Modern technological advancements such as photoacoustic imaging, optical coherence tomography, diffuse optical tomography and ultraviolet dermatoscopy approaches seek to provide a noninvasive diagnostic approach with minimal destructive power [10]–[12].

Diffuse Reflectance Overview

A unique biophotonic approach relevant to this dissertation is diffuse reflectance spectroscopy (DRS) [13]. This is a noninvasive technique that works in conjunction with quantitative models by extracting optical properties from tissues with the goal of characterizing tissues and ultimately diagnosing disease [14]. In DRS, incident light enters a substance while scattering and absorbing molecules, until it reflects out of the tissue as shown in Figure 2-3. The migration of light through a substance depends on the

wavelength of light and optical properties of the tissue sample, including layer thickness, absorption, scattering coefficient, scattering angle probability and the tissue refractive index [15]. Depending on the distance between the source and detector of the DRS, there can be different information observed about the tissue. It has also been well established that the optical properties of tissue change during the advancement of different diseases which makes DRS a valuable diagnostic approach.

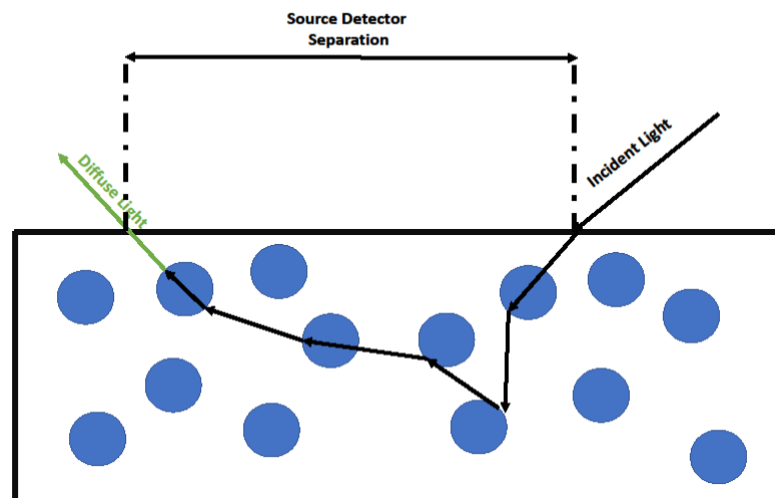


Figure 2-3. Tissue Diffuse Reflectance.

DRS system components consist of a light source, fiber optic probes and a spectrometer [16]. Light sources are dependent on the application; however, basic DRS systems use a halogen light source. Halogen bulbs have a wavelength specification range from approximately 400 nm to 900 nm; however, in recent years, light sources include broadband diodes and LEDs. This is standard when taking measurements of many

chromophores specific to transcutaneous measurements, such as hemoglobin, melanin and bilirubin. The fiber optic probe acts as a guide for the light source and the collection of diffuse reflected light. Common fiber optic probes are designed with either a centered light source surrounded by coaxial rings of collection fibers or a ring of collection fibers surrounded by light source fibers. The source-detector separation configured in each fiber probe can serve a valuable purpose of collecting photons whose mean-pathlength through the tissue increases with increasing spatial offset [17]. Thus, the careful design of detection source-detector offset can result in collection of depth dependent information from a specific subsurface zone within the tissue, while more collection fibers with multiple source detector offsets can result in diffusely reflected signals with a variety of depth-dependent profiles [18].

Various approaches have been developed to translate spectrally resolved data into measurements that provide relevant identifiers to different diseases [19]. These approaches include forward and inverse Monte Carlo simulations of model look up tables that use prior knowledge of absorption and scattering coefficients to estimate tissue composition [20]. Other models utilize machine learning techniques such as neural networks or principal components to associate spectrally measured results with specific diagnoses. Another approach is to use mathematical models that take in multiple biological parameters for the diagnosing of the disease. This is done by utilizing the DRS signals collected at a variety of specific wavelengths directly associated biological markers of relevance.

Diagnosis of disease can benefit from either qualitative or quantitative assessment. DRS has been shown to provide benefits in both cases. DRS has been used qualitatively to determine differences between tissue types and binary diagnosis (benign or malignant) [21]. It has also been used as a medical monitoring technique in cases such as pulse oximetry [22]. Pulse oximeters are used to measure the oxygenation of a patient's arterial blood, which is a continuous variable. Clinicians depend on accurate measurements of the oxygenation of blood as it offers valuable information about the progression of varying severe conditions. For DRS systems such as pulse oximetry where accuracy is crucial to the diagnosis, mathematical models are preferred due to spectral overlapping of oxygenated and deoxygenated hemoglobin. Many pulse oximeters are equipped with multiple light sources that measure both chromophores in conjunction with a mathematical model.

Traditional DRS systems are commonly configured with a single point source-detector setup [23]–[25]. While this configuration is well-established for many clinical platforms, limitations persist in the accuracy and specification for diagnosing diseases [26], [27]. In many cases, clinicians need to survey a large area; and traditional DRS techniques make this process subjective and error-prone. Techniques such as spatial frequency and hyperspectral imaging has expanded DRS to a 2d imaging platform [28]–[32]. This not only expands the field of view of DRS, but has also shown to increase the resolution of the spectra. While this is a fairly new concept, it opens the door for future uses of 2d DRS imaging to address a multitude of conditions.

Overview of Skin Structure, Composition and Optical Properties

OD approaches are very common in many healthcare practices aiding in the identification of different diseases using skin measurements [33]–[35]. The skin is the largest soft tissue organ and is composed of 3 different layers as seen in Figure 2-4. The outer most layer, the epidermal layer, acts as one of the first lines of protection against foreign invaders, toxins and ultraviolet light [36], [37]. This layer also houses pigment cells called Melanocytes, which give the skin its color. The activation of melanocytes produces melanin pigment which act primarily as optical scattering chromophores. The dermal layer is located directly underneath the epidermal layer. This layer houses collagen, hair follicles, sweat glands, blood vessels and nerves. It is responsible for thermal regulation through sweating and nerve sensation to report changes in temperature to the brain. The chromophores in this layer act as primary absorbers of light. Below the dermal layer lies the hypodermal layer, where subcutaneous fat and larger blood vessels lie.

Optical properties from the skin are influenced by its composition, such as skin thickness, the concentration of blood, melanin and bilirubin. Accurate measurements of the optical properties can be crucial for the evaluation of neonates diagnosed with jaundice.

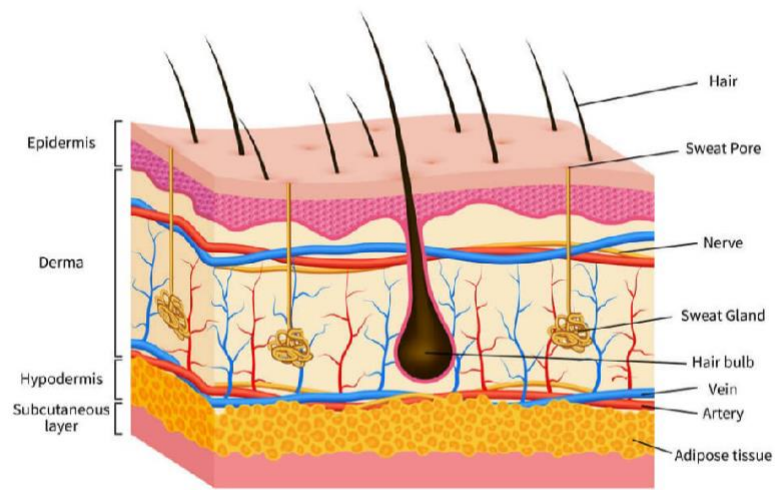


Figure 2-4. Skin Layers [38].

Neonatal Jaundice

Neonatal jaundice (NNJ) is one of the most common neonatal conditions that requires immediate attention within the first week of a neonate's birth [39]. In some cases where the skin has less pigment, this condition can be visually assessed by the yellowing of the skin or eyes (Figure 2-5), due to the circulation of bilirubin in the neonate's blood streams. Bilirubin is a byproduct of the catabolism of red blood cells. Catabolism of red blood cells occurs when these cells need to be broken down and discarded to accommodate the creation of newer blood cells. When a neonate is born, there is a transition period between when the mother carried out the heavy lifting of catabolism for the neonate prior to birth and the neonate needing to break down red blood cells on its own after birth.

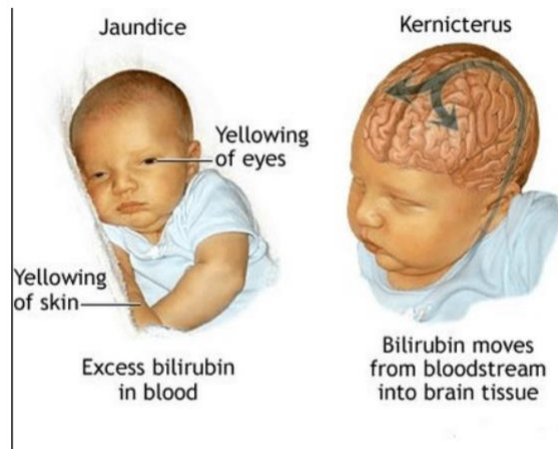


Figure 2-5. Jaundice in Neonates [40], [41].

While this is generally harmless, high concentrations of bilirubin in the blood stream can develop into hyperbilirubinemia [42]. This buildup of bilirubin is due to either an overproduction or slow elimination of bilirubin. Slow elimination of bilirubin can either be due to immature development of the liver and kidney organs, which help remove bilirubin from the body, or a malfunction of these organs [43].

The danger of high levels of bilirubin, or hyperbilirubinemia, is that bilirubin is neurotoxic and has the ability to cross the blood brain barrier [44]. Without treatment, a neonate can develop kernicterus (permanent brain damage) and may even lead to death if kernicterus persists. While the persistence of NNJ is dangerous if left unchecked, this condition is treatable through blue light phototherapy. In extreme hyperbilirubinemia cases, they can be treated with a blood transfusion. Thus, it is crucial to diagnose this condition as early as possible to increase the chances of a positive prognosis.

Management of NNJ

It is routine to screen for bilirubin levels 24 hours after birth in healthcare systems in high-income countries. Physicians can then make decisions about treatment options for the patient based on the screened bilirubin levels [45]. However, in low- and middle-income countries (LMIC) where the instances of NNJ are higher (Figure 2-6), the management approaches for NNJ are limited [46]. This is partially due to an increased amount of home births in LMIC, which ultimately leads to higher instances of extreme hyperbilirubinemia. Limited accessibility to screening devices forces approaches such as icterometers on LMIC. Icterometers work by blanching the neonate's skin and comparing the yellowness to a scoring ruler as shown in Figure 2-7A. However, this device offers no quantitative measurement and is highly subjective, especially in highly pigmented infants as shown in Figure 2-7B. Subjective measurements from this device create challenges when attempting to make consistent clinical decisions.

Total serum bilirubin (TSB) is the gold standard for the measurement of bilirubin levels. However, this approach is invasive and can expose the neonate to the risk of infection, in addition to the long wait times for bilirubin level results to be reported to physicians. This can potentially lead to prolonged exposure of high bilirubin levels in neonates that have been diagnosed with jaundice.

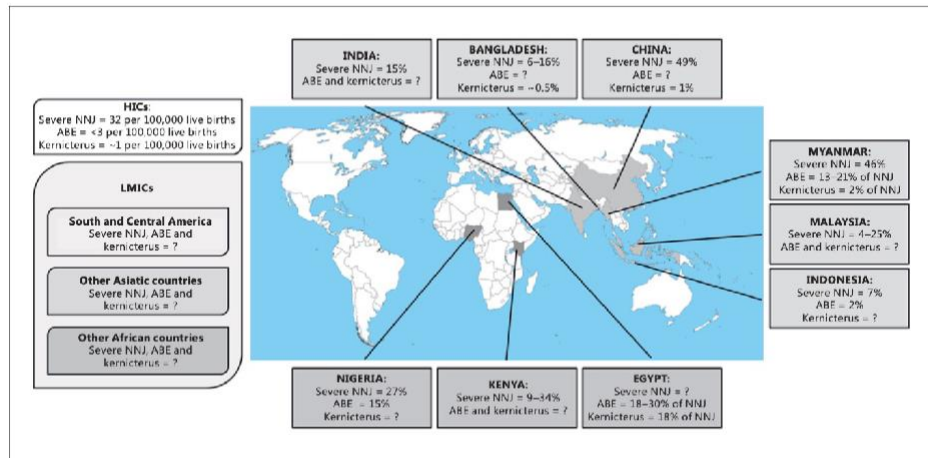


Figure 2-6. Global Impact of NNJ [40], [41].

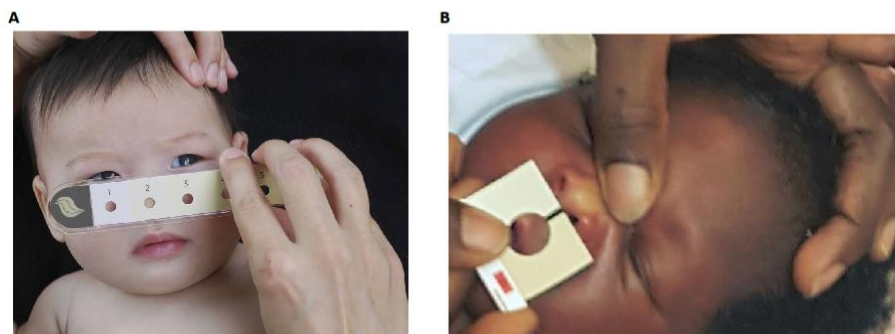


Figure 2-7. Icterometry in Neonates [40], [41].

Clinical Transcutaneous Bilirubinometry

The first few months of a neonate's life are crucial to their development; thus, screening approaches for NNJ need to be accurate and provide quick results. An alternative approach to screening for NNJ is the use of an optical diagnostic (OD) approach known as Transcutaneous Bilirubinometry (TcB) [47]. OD techniques are advantageous because they are noninvasive and provide instantaneous results.

Clinical TcB is performed by placing the device in direct contact with the neonate's skin, preferably at the sternum, forehead, or interscapular areas as shown in Figure 2-8A. TcB devices utilize the biophotonic phenomena known as diffuse reflectance (DR), a technique that occurs when emitted light scatters and absorbs inside a medium and scatters out of the medium away from the point of entry of the emitted light as shown Figure 2-8B [41].

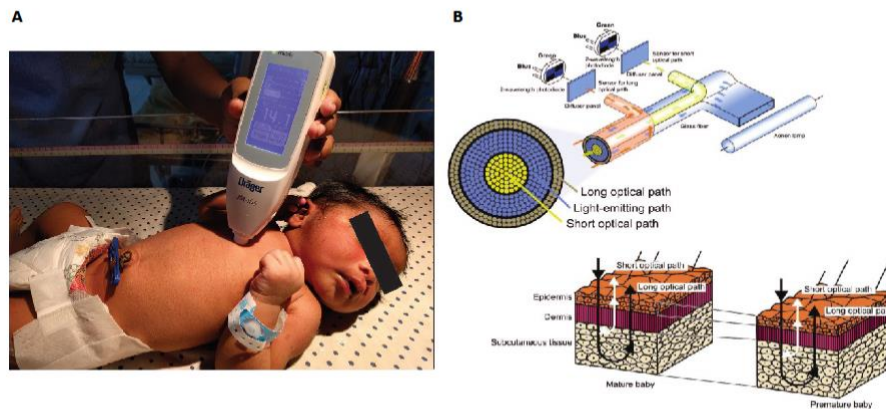


Figure 2-8. Transcutaneous Bilirubinometers [40], [41].

Similar to most OD approaches, clinical TcB devices utilize the collected DR measurements paired with multivariate linear regression (MLR) models. MLR models depict the relationship between independent variables (predictor variables) that make up the unique composition of variability in the dependent variable (prediction variable) simultaneously. Utilization of independent variables with low collinearity are crucial for developing strong and generalizable models.

Each unique OD approach has its own distinctive MLR model. The challenge with OD approaches based on tissue diffuse reflectance is that the independent variables have high collinearity, which leads to poor outcomes in prediction models. Clinical TcB devices such as the JM-103 and Bilicheck are designed with the intent of reducing the collinearity between their independent variables for more generalizable models [41]. The JM-103 independent variables are diffuse reflectance signals collected at short or long pathlengths and wavelengths at 470 nm, 550 nm and 650 nm. The Bilicheck's independent variable inputs are diffuse reflectance signals collected at one pathlength and 7 wavelengths.

While clinical TcB devices are influential in improving the management of NNJ, limitations of underestimation in bilirubin measurements persist. Clinical TcB devices have shown reduced accuracy during and after phototherapy treatment. This may be due to morphological aging that happens when skin is exposed to phototherapy [48]. Results have shown better correlation to Total Serum Bilirubin (TSB) levels when skin is protected from phototherapy treatment. Issues of reduced accuracy in clinical TcB also persist in cases where neonates are born premature or have increased pigmentation in

their skin [49]. This reduced accuracy suggests poor MLR prediction models with independent variables that have high collinearity. This high collinearity appears to be due to a limitation in probing layer-dependent chromophore melanin. Lastly, clinical TcB approaches are also expensive, which further reduces the accessibility of these devices in LMIC.

Due to increased accessibility, mobile phones have become a popular platform sought after by researchers to transform them into OD devices [50]. Mobile phones are pre-equipped with a flash and camera, which are the basic components for most OD approaches. A few groups have shown how to transform the mobile phone into unique TcB devices. The Bilicam is the first to be created by using camera-based color correction cards, along with images of neonatal skin collected with the cell phone camera as inputs to their MLR model (Figure 2-9A) [51]. This technique has had success in demonstrating feasibility in multiple clinical studies. In Figure 2-9B, a research group has combined a dermatoscope with a mobile phone device. A dermatoscope is typically used by dermatologists to illuminate a patient's skin to aid in skin cancer screening [52]. With the addition of a single filter, this group was able to demonstrate feasibility in a small pilot study through images collected by a mobile phone. Another group from Japan utilized Bluetooth capabilities from the mobile phone to send a signal from the device that shines blue light into the skin and collects diffuse reflectance signals when placed on the neonate's forehead (Figure 2-9C). All of these approaches demonstrates unique transformation of the mobile phone as an OD device. However, due to early stages of

development, these approaches either lack accuracy, are limited to Caucasian neonates, small sample size or not validated for LMIC.

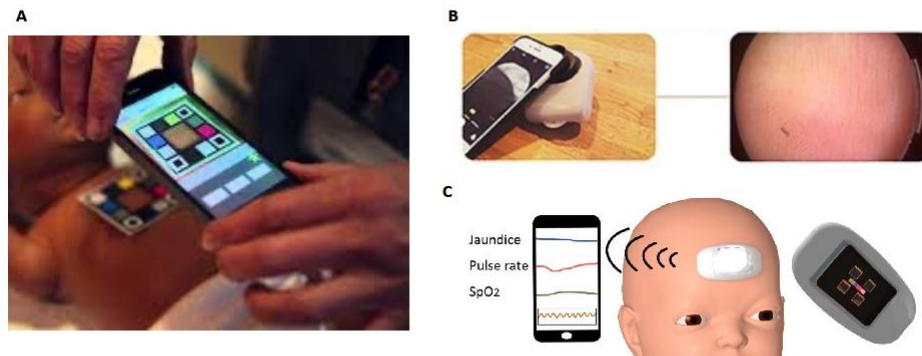


Figure 2-9. Mobile Phone-Based Bilirubin Devices [51]–[53].

Next generation bilirubinometry may be possible with point of care style devices. Technologies based on diffuse reflectance light-matter interaction offer promising opportunities for noninvasive transcutaneous measurements of bilirubin and are direct descendants of clinical TcB devices. Adaptions could be made to address known chromophore issues with overall DRS signals, such as the impacts due to increased melanin. This may lead to improvements of management systems for neonatal jaundice in LMICs.

3. DEVELOPMENT OF A MOBILE PHONE CAMERA BASED TRANSCUTANEOUS BILIRUBINOMETER FOR LOW-RESOURCE SETTINGS

Abstract

Newborns in high-income countries are routinely screened for neonatal jaundice using transcutaneous bilirubinometry (TcB). In low-and middle-income countries, TcB is not widely used due to a lack of availability; however, mobile-phone approaches for TcB could help expand screening opportunities. We developed a mobile phone-based approach for TcB and validated the method with a 37 patient multi-ethnic pilot study. We include a custom-designed snap-on adapter that is used to create a spatially resolved diffuse reflectance detection configuration with the illumination provided by the mobile-phone LED flash. Monte-Carlo models of reflectance from neonatal skin were used to guide the design of an adapter for filtered Red-Green-Blue (RGB) mobile-phone camera reflectance measurements. We extracted measures of reflectance from multiple optimized spatial-offset regions of interest (ROIs) and a linear model was developed and cross-validated. This resulted in a correlation between total serum bilirubin and mobile-phone TcB estimated bilirubin with a $R^2= 0.42$ and Bland-Altman limits of agreement of +6.4 mg/dL to -7.0 mg/dL. These results indicate that a mobile phone with a modified adapter can be utilized to measure neonatal bilirubin values, thus creating a novel tool for neonatal jaundice screening in low-resource settings.

Introduction

Neonatal jaundice (NNJ) is a common condition clinically associated with some degree of yellowing of the skin and eyes that typically self-resolves in the first week after birth [54]. NNJ is characterized by an elevation of serum bilirubin levels driven by underdeveloped bilirubin metabolism. However, prolonged and extreme hyperbilirubinemia (EHB) is problematic due to bilirubin's neurotoxicity and can ultimately lead to kernicterus, severe neurosensory deficit and even death [44].

EHB-related neonatal mortality in low- and middle-income countries (LMIC) is reported to be approximately 638 infants per 10,000 births, compared to 3.7 infants per 10,000 births in high-income countries [55]. In LMIC, poor EHB-related outcomes arise from a multitude of factors, including increased underlying prevalence of genetic conditions such as glucose-6-phosphate dehydrogenase (G6PD) deficiency and hemolytic diseases, increased prevalence of risk factors such as sepsis and low birth weight, high-rates of non-institutional delivery resulting in delayed care, as well as inconsistent availability of laboratory based diagnostic testing and phototherapy treatment units [56]–[59]. While the clinical reference for diagnosis is gold-standard blood testing of total serum bilirubin (TSB), inconsistent availability of facilities and supplies remain a problem due to high rates of home births in LMIC. Therefore, simple visual examination of skin blanching is used for newborn jaundice screening, despite limited precision and inferior ability to predict neurological injury from EHB in comparison to TSB [59]–[61]. Low-cost point-of-care blood testing solutions can potentially reduce barriers to

quantitative assessment of bilirubin that exist in LMIC [62]–[65]; however, a noninvasive approach could be a desirable alternative for early screening.

Transcutaneous Bilirubinometers (TcB) are a widely used optical reflectance technique that performs screening measurements near bilirubin’s absorption maxima at 460 nm along with at least one additional reference measurement above 500 nm to normalize for optical variations in tissue including perfusion, pigmentation and scattering [66], while also detecting two distinct spatially offset detection channels with different depth-dependent biases [67]. Over the last 20 years, TcB has become an important element in a systematic approach for universal screening newborn’s risk for EHB in high-income countries [68]–[70]. Infants identified as at-risk subsequent diagnosis can be confirmed via TcB, appropriate treatments are administered in a timely fashion and instances of chronic bilirubin encephalopathy (CBE) and EHB-related deaths are extremely rare in high income countries such as the United States [55], [71]. Expanded adoption of TcB in LMICs has been proposed but the cost of currently available TcB devices remains an obstacle. As a result, development of low-cost and mobile phone-based approaches to estimate serum bilirubin levels have been proposed [12], [51], [72]. In particular, a mobile phone-based platform offers a strong potential for integration with communications networks for coordination of care, healthcare data management and real-time patient monitoring [73]–[75].

In this manuscript, we report the development of a mobile phone-based TcB device. The approach mimics clinical TcB by directly measuring a spatially-offset diffuse reflectance in direct contact with the infant’s skin. Monte-Carlo models of reflectance

from neonatal skin were used to guide the design of an adapter for filtered Red-Green-Blue (RGB) mobile phone camera reflectance measurements. A pilot study was performed across two sites in the United States and Nigeria in order to include infants with a wide range of pigmentation; and a generalized linear model was developed using multiple spatial offset regions of interest (ROIs) across the RGB reflectance channels. Results indicate that this approach holds promise for mobile phone-based approaches for estimating bilirubin in neonates. While there are multiple mobile phone based TcB devices, no devices to our knowledge have been shown to utilize multi-band filters in conjunction with a smart ROI search system and include data from African neonates.

Materials & Methods

Monte-Carlo Modeling of a Smartphone Based TcB Device

The principle of the mobile phone TcB device reported here is inspired directly from clinical TcB. Monte-Carlo (MC) modeling of photon migration in tissue has been a well-suited approach for theoretical investigation of diffuse reflectance in TcB and has provided valuable insights into the influence of pigment, scattering, illumination/collection geometry and light source selection [76], [77].

The overall design concept was to create an adaptor that could be placed over the phone's LED light source and camera module. Monte Carlo simulations were used to guide illumination/collection geometry design and optimize the collection of a wide range of reflectance intensities observed when capturing spatially resolved images at

multiple spatial reflectance offsets seen across the 400-700 nm spectral range. Our preliminary data suggested a large mismatch in reflectance across the blue and red channels leading to an insufficient blue channel reflectance signal at appropriate spatial offsets [78]. We created MC models for diffuse reflectance of neonatal skin with illumination/collection parameters that matched the proposed geometry of the mobile phone camera adaptor, and then used the simulation outputs to determine the relative benefit that a reduction in source-detector separation would have on improving disparities expected in red/blue channel reflectance. A physical design of the prototype smartphone adaptor, along with a representative MC simulation of photon flux in the skin, is shown in Figure 3-1A.

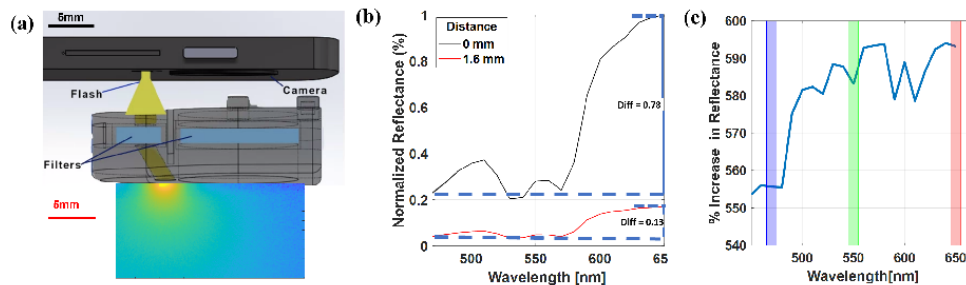


Figure 3-1. (A) 3D physical model of the mobile phone TcB design which depicts illumination through the device. An MC photon fluence map depicts modeled light distribution in neonatal skin. (B-C) Monte Carlo simulation results: (B) Normalized reflectance for two configurations and (C) Percent increase of reflectance from 0mm to 1.6mm configurations in the red, green and blue filtered channels.

Monte-Carlo modeling was performed using the Monte Carlo eXtreme (MCX) platform [79], [80]. A generalized tissue optical model was configured to simulate neonatal skin, with parameters related to skin thickness, scattering and chromophore concentration and extinction informed from prior work [76], [77]. Melanosome fractional volume was set at 10% to determine model performance in darkly pigmented skin, where overall signal intensities are lower [77], [78]. The optical illumination and detection configuration in MCX was directly informed by both the physical and optical specifications of the LG Nexus 5 Android smartphone and the proposed adaptor, including LED-to-camera offset edge-to-edge offset, illumination spot size, detector size and imaging optics. Two optical configurations were simulated; (1) the offset between the proximal edge of the illumination beam and the proximal edge of the camera field-of-view was set to 1.6 mm, and (2) the offset was reduced to 0 mm. In both configurations, the adaptor thickness was set to 10 mm, and modeled spectral diffuse reflectance from 400-700 nm was determined based on inclusion of all diffusely reflected simulated photons within the acceptance angle of the imaging optics arising from within the 9mm x 12 mm field of view (FOV). FOV was verified through empirical measurements with a microscopy calibration grid. Thus, the source-detector offset from the center of the source to the center of the image FOV for the two configurations is 7.5mm and 9.1mm. After running the MC simulations, modeled spectral normalized diffuse reflectance is generated for the two configurations (Figure 3-1B), and the percent reflectance increase differences in spectral intensities were compared across each RGB color channel (Figure 3-1C). Results of these simulations indicate differences in the relative magnitude of

color-channel dependent changes in detected reflectance for the two flash-detector offsets, and informs any potential reduction in the range of reflectance values measured across channels.

Mobile Phone TcB Optical Adapter

Based on the results of the MC models, an adaptor (shown in Figure 3-2A) was developed to be placed between the mobile phone (LG Nexus 5) camera/LED and the infant's skin, with the purpose of redirecting LED illumination to a confined spot with minimal spatial offset from the camera's field of view and housing triple-band pass optical filters for improved spectral isolation of RGB measurements (Figure 3-1A).

A 10 mm thick prototype adapter was 3D printed (Connex 3 Object 500 3D printer, Stratsys Ltd.) using black material (Vero Black, Stratsys Ltd.) in order to reduce the intensity of light that may transmit through the plastic. The adapter (Figure 3-2A) was fixed to a generic snap-on protective case and aligned over the camera and flash.

Although the 10 mm thickness of the adapter is shorter than the minimum working distance, a measurement of the defocused edge response resulted in a 90% to 10% width corresponding to approximately 1.4 mm over the 12 mm image width. A 2 mm pinhole on the phone-facing side of the adapter served to reduce the half angle of the LED from approximately 41 degrees to 21 degrees to preserve the spectral performance of a triple-band pass filter (IDEX Semrock FF01. D=5mm) with passbands at 474 +/- 10nm (blue), 554 +/- 10nm (green) and 635 +/- 10nm (red). After the filter, an angled 2mm channel directs the light towards the camera field of view, with a minimum offset that is limited

by performance of the 3D printer. The spatially offset diffuse reflectance is then collected via a separate optical path that includes a notched space for a second, larger triple-band pass filter (D=10 mm) with identical spectral profile. The adapter containing band-pass filters attached with the smartphone is shown in Figure 3-2B. All components, including the 3D print material and filters were selected based on their resistance to degradation from simple disinfectant with 70% ethanol protocols [81], [82].

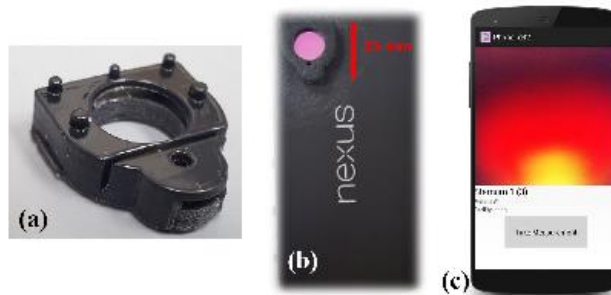


Figure 3-2. Implemented Smartphone-Based TcB Device: (A) 3D printed adapter which guides light towards skin and house the band-pass filters. (B) Device attached to the phone casing with filters. (C) Smartphone application interface while taking a measurement from skin.

Diffuse Reflectance Measurements and Calibration

A custom mobile application was developed in order to configure mobile phone image acquisition, as well as guide users through calibration and clinical measurements. The basic interface of the smartphone application during image capturing is presented in Figure 3-2C. Image data is configured to be saved without pre-processing or compression

in raw 16-bit format in order to ensure the data could be used for quantitative measurement of reflectance. Camera acquisition parameters were fixed, including focus, exposure time and ISO/gain. Each measurement consisted of acquisition of 3 successive tissue reflectance images with exposure time of 400 ms and ISO of 4500, along with a paired set of 3 dark background images collected with the LED off. In this study, 3 replicate sets of measurements were collected from each infant to ensure unexpected clinical scenarios, such as sudden movements, did not reduce enrollment yield.

Calibration was performed by measuring a custom calibration standard consisting of a 25x25x5 (thick) mm High-Density Polyethylene (HDPE) white plastic block housed in a Vero Black casing using an identical sequence of reflectance (LED on) and background (LED off) image acquisitions. Paired calibration measurements were collected for each patient enrolled.

Human Subjects

Measurements were collected utilizing the mobile phone TcB device from 37 neonates (30 from Vanderbilt University Medical Center (VUMC), Nashville, TN, USA and 7 from Aminu Kano Teaching Hospital (AKTH), Kano, Nigeria). Healthy infants between 24-72 hours postnatal age were considered eligible for this study. Exclusion criteria included infants born with known or estimated gestational age less than 32 weeks, weighed under 1500 grams, or prior phototherapy. Each mobile phone measurement was obtained within 30 minutes of a blood sample used to obtain TSB. Written consent was obtained from all parents, and all studies were performed in accordance with the

institution's human subjects research approvals (VUMC IRB130471 and AKTH EC1390). All measurements were collected using the smartphone in direct contact with the sternum of the infant while minimizing in rooms where bright ambient lighting was minimized. Our device requires that all measurements be made with the device placed flat and flush against the skin. The forehead has varying curvatures between neonates, while the sternum location has less variability in curvature. This allows for more uniform and consistent measurements taken with our device. The demographic distributions of the neonates are provided in Figure 3-3A. The distribution of TSB values obtained for all the neonates are shown in Figure 3-3B, indicating a right-skewed, non-normal distribution characteristic of newborn TSB, with a majority of values between 5-10 mg/dL and some infants with elevated values as high as 23.7 mg/dL.

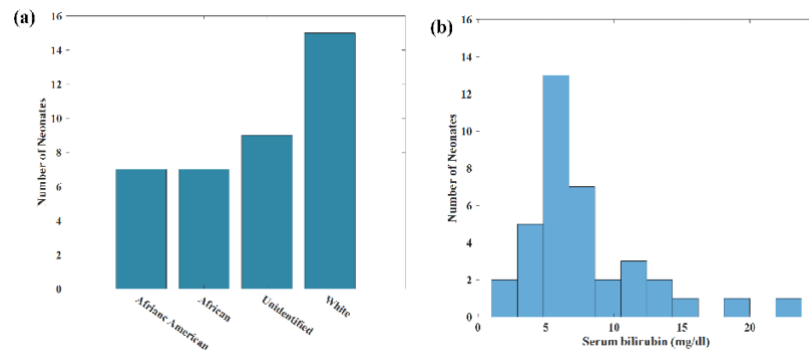


Figure 3-3. Human Subject Study: (A) Number of neonates used in the study. (B) Serum bilirubin distributions of neonates where majority of TSB values are clustered around 5-10 mg/dL.

Image Pre-Processing

Raw images were extracted from the mobile device and converted to Digital Negative (.dng) format with an Adobe DNG Converter prior to import in MATLAB (Mathworks) for processing. DNG images were demosaiced, resulting in Red, Green and Blue (RGB) and resized to a quarter of the original image to reduce the data size for analysis. All images were processed through a multivariate k-nearest-means outlier detection algorithm [83], which was used to identify sets of images that contained poorly performed measurements (i.e. infant motion, device non-contact). Once the outliers were removed, each set of images (sternum and calibration images) was averaged, resulting in one final image each for sternum reflectance, sternum background, calibration reflectance and calibration background was associated with each patient. Reflectance images were background subtracted and normalized by calibration images in order to produce a single RGB-calibrated reflectance image for each patient. Representative patient RGB image data used for subsequent analysis is shown in Figure 3-4 (A-C).

Development of Region of Interest (ROI) Based Generalized Linear Model

Optical estimation of bilirubin levels is classically informed through creation of linear regression models of the reflectance from unique spectral and spatial channels against matched TSB values [67]. In our mobile phone TcB device, the pre-processed images represent a spatially resolved map of tissue diffuse reflectance, and thus a linear model can be created similar to classical TcB using multiple unique spatial offset within each RGB spectral image channel. Unlike conventional

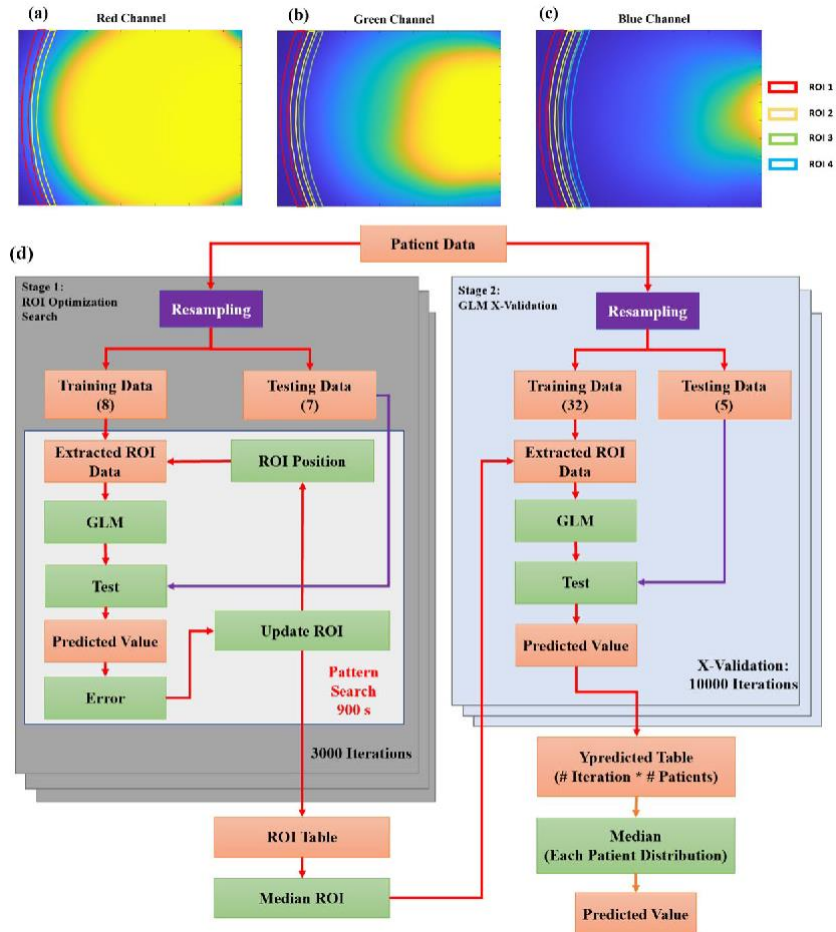


Figure 3-4. Two-Stage ROI-based GLM. Images and ROI initial positions for (A) Red (2 ROIs), (B) Green (3 ROIs) and (C) Blue (4 ROIs) channels. (D) The overview of the two-stage ROI optimization and model cross-validation algorithm. Input, intermediate and output data depicted as orange boxes; primary operations as purple boxes and secondary operations as green boxes.

TcB, where physical detectors placed at unique offsets define independent spatial channels, collection of images of diffuse reflectance produces a spatially resolved reflectance map and offers the opportunity to define multiple spatial offset channels uniquely in each RGB spectral channel. In order to determine appropriate placement of the spatial offset channels and to develop the corresponding linear model, a two-stage approach was used. In the first stage, a bounded pattern search optimization algorithm was used to identify the placement of specific spatial offset channel's regions of interest (ROI). In the second stage, the reflectance within the ROIs was used to develop and cross-validate a generalized linear model (GLM) to estimate TSB. A block diagram depicting two-stage model development and cross-validation is shown in Figure 3-4D.

Based on the right-skewed non-negative distribution of the TSB values (Figure 3-3B) along with the resulting limited number of infants enrolled with TSB values greater than 15 mg/dL, fully randomized selection of patients to include in training subsets would result in high likelihood models constructed in individual cross-validation iterations were informed with data from infants with TSB tightly clustered between 5-7 mg/dL, and oftentimes no subjects greater than 12 mg/dL, while the clinically relevant range of newborn bilirubin levels from 0-20 mg/dL.

In order to account for this enrollment-dependent limitation in the ROI optimization stage, the full data set was first sorted according to TSB values and then divided into 4 different ranges (0-5mg/dl, 5.01-10 mg/dl, 10.01-15mg/dl and 15.01-25 mg/dl). Training data sets consisted of randomized resampling of 2 patients each across the 4 TSB bins to total 8 uniformly sampled patients across the full TSB range. The ROI

test sets were then selected from the remaining pool of patients with 2 patients from the first 3 ranges and the 1 remaining patient left in the highest TSB range (only 3 enrollees had TSB levels greater than 15 mg/dL) to total 7 patients. This resampling approach ensured uniform distributions to guide ROI optimization despite limitations in the sample sets distribution. A bounded pattern search algorithm implemented in the MATLAB optimization toolbox (Mathworks) was used to optimize ROI placement [84]. Here, the spatial offset areas are arc-shaped regions of interest (ROI) in each spectral (RGB) image frame defined based on their position, radius and width. Initial conditions for 4 ROIs in the blue channel, 3 ROIs in the green and 2 ROIs in the red (Figure 3-4A-C). The number of ROIs per channel was selected based on the relative amount of unsaturated area in each image channel's FOV, where the blue channel had the most and the red channel had the least. The pattern search algorithm uses the mean values within the ROIs as the observed variables for a gamma distribution (non-negative constraint) based GLM to predict TSB [85]. The pattern search algorithm aims to iteratively adjust the positions of the ROIs in order to optimize the sum square error of the GLM over a duration of 900 s. After completion of the pattern search, the ROIs are stored in a table and the optimization was repeated over 3,000 different resampled iterations, resulting in 3000 different estimates of ROI positions. The median of each ROI position was calculated to determine the 9 different ROIs which were served as the output of stage 1 and were used for further analysis.

After the final ROI positions were determined, the second stage of the routine performed cross-validation of the GLM's ability to predict the bilirubin values from

patient images. Here, the patient images were sorted by bilirubin values and divided into 5 different ranges (0-3.5 mg/dl, 3.51-6.5 mg/dl, 6.51-10 mg/dl, 10.01-15 mg/dl and 15.01-25 mg/dl). In each cross-validation, 1 patient was selected randomly from each of the ranges to create a 5 patient test set. The remaining 32 patients were considered for the training set. Using the median ROI positions measured from the initial pattern search-based algorithm, ROI data were extracted from the training data to create a GLM. The GLM's performance was evaluated on the testing dataset. This process was carried out for 10,000 cross-validations. After running 10,000 cross-validation, a table of predicted values was generated containing a distribution of predicted values for each patient. Then, the median of each patient's predicted values was taken. Cross-validation using this approach for resampling training and testing data over many iterations [86], [87] can then be used to produce a robust composite estimates of the model's performance.

A correlation plot for predicted bilirubin values vs. TSB and a Bland-Altman plot were generated to report model performance, bias and limits of agreement. In addition, the final ROI parameters were calculated as the mean positions across all cross-validations. The final median ROIs calculated across all cross-validations are presented in Figure 3-5(A-C).

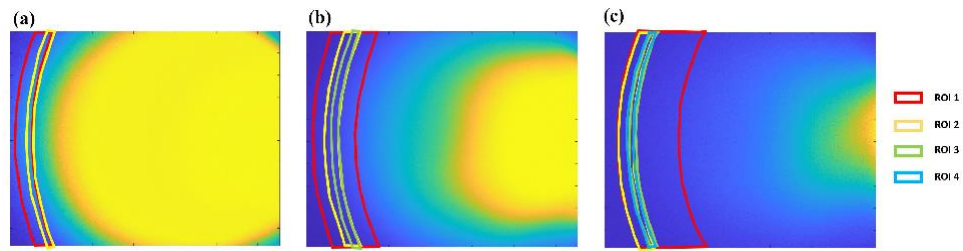


Figure 3-5. Images with final ROI positions for (A) Red (2 ROIs), (B) Green (3 ROIs) and (C) Blue (4 ROIs) channels generated after stage 1 ROI optimization.

Results

Monte Carlo Model

A MCX model was used to compare the effect of reducing the illumination-detector offset on the collected diffuse reflectance signal. Figure 3-1B-C) represents the impact of source detector offset on diffuse reflectance intensities across the spectral range. In Figure 3-1B there is a clear increase in measured reflectance when the source to detector separation is decreased from 1.6 mm to 0 mm. In addition, the modeled spectra indicate blue channel reflectance to be the lowest, while red channel reflectance to be the highest. The difference between reflectance intensities from blue to red is calculated as 0.13 for the 1.6 mm configuration vs. 0.78 for 0 mm configuration. Figure 3-1C also shows percent increase in the reflectance for the 0 mm vs. the 1.6 mm configuration. Note that while reducing the offset increases the weak blue channel reflectance, it results in a slightly greater increase in the red channel.

Mobile Phone TcB Design and Characterization

A prototype and implemented mobile phone TcB device is illustrated in Figure 3-1A and Figure 3-2B. The Mobile Phone TcB device is directly mounted over the flash and camera of the LG Nexus 5 mobile phone. Along with the adapter, the mobile phone TcB app is used to help users capture images of the neonate's skin. The light from the flash is then filtered and enters the skin at a 30 degree angle with a 0 mm source to detector separation.

Pilot Study Results

The ability to measure bilirubin levels was evaluated in a pilot study conducted at Vanderbilt University Medical Hospital (VUMC) and Aminu Kano Teaching Hospital (AKTH). Figure 3-3A represents a demographic breakdown of the 37 neonates that participated in this study. There are 14 African or African American neonates, 15 Caucasian neonates and 8 race unclassified neonates. TSB and mobile phone TcB measurements were collected from each patient. The measured bilirubin TSB levels complemented the clinical bilirubin range from 0-25 mg/dL, with the majority ranging between 5 and 10 mg/dL. Figure 3-6A shows a correlation for the predicted TSB levels from the mobile phone TcB device with an R^2 value of 0.42 ($p=1.41 \times 10^{-5}$). The Bland-Altman plot in Figure 3-6B shows a mean difference of -0.28 mg/dL ($p=0.62$) between the mobile TcB device and TSB measurements and 95% Limits of Agreement (LOA) are 6.4 mg/dL to -7.0 mg/dL (range between the upper and lower limits of LOA equal to 13.4

mg/dL). The root-mean-square error (RMSE) for the range between 0-10 mg/dl is around 2.13 mg/dl, whereas the RMSE in the range between 10.01-25 mg/dl is 6.05 mg/dl. This could be since the dataset had fewer neonates over 10 mg/dl to create the linear model and test it. These results indicate the ability of the smartphone-based TcB device to estimate TSB values in a racially diverse group of neonates.

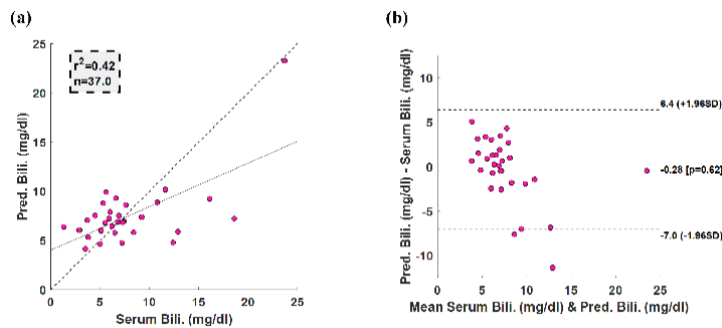


Figure 3-6. Linear regression statistics (A) Correlation and (B) Bland-Altman of the mobile phones predicted bilirubin values vs. TSB values (n=37 patients).

The root-mean-square errors (RMSE) for 3 different skin groups (light or dark skin) were calculated from the resulted predicted values. In light skinned infants (n=15), the RMSE was 4.77 mg/dL; whereas, in case of dark skinned neonate's (n=14), the RMSE was 2.05 mg/dL. However, a two sided t-test showed that error in dark skinned infants is not significantly different than white infants.

Discussion

Extreme hyperbilirubinemia (EHB) contributes up to 14% of neonatal deaths and causes significant amount of neurological sequelae in low-resource settings [60].

Reducing the global burden of EHB in LMIC is a complex problem, including challenges in the lack of genetic screening, maternal education, adoption of universal practices for newborn screening and expansion of availability of phototherapy [88]. A low-cost mobile phone-based approach to TSB estimation can take advantage of the expanding access to smartphones across low-resource and rural areas in LMIC [89] and has substantial potential to improve screening practices if effective. Moreover, the connection of data and information services through smartphones offers the potential for coordination of treatment services for jaundiced infants requiring care in remote areas. Here we describe the development of a mobile phone-based approach for TcB measurement that uses an optical adaptor fitting commercially available protective mobile phone cases. The adaptor design enables collection of spatially resolved images of diffuse reflectance with an offset illumination spot through a set of optical filters. The total cost of the adaptor, not including the mobile phone, is approximately less than \$1,000 US dollars (Filters \$400 US dollars each and 3D printed material \$20 US dollars). The cost of the commonly used Drager Jm-105 Jaundice meter can be priced at \$1,100 US dollars. Although the filters used in this adaptor are scientific grade coated glass substrate, low-cost, durable, coated plastic optical filters allow production of similar adaptors for less than \$50 US dollars [90]. Alternatively, spectral filters with reduced transmission in the red channel could be used to reduce the difference between reflectance from blue and red spectral channels to

expand the spatial range of usable data by exposure balancing. The use of a passive adaptor, in combination with the novel approach of extracting multiple spatial and spectral ROI reflectance channels within the RGB image data, offers a promising and unique approach for TSB estimation in low-resource settings.

The mobile phone-based approach reported here produced an estimation of TSB within 6.4 to -7.0 mg/dL, with a bias of -0.28 mg/dL (Figure 3-6B). These results are comparable to, but not as positive as, previously published results of TcB-TSB agreement in large, multi-ethnic study populations, which have a maximum span of the reported LOAs falling between approximately 4 and -6.0 mg/dL and biases between 1.6 and -0.8 mg/dL [91]–[94] This suggests promise that with further development, mobile-phone based approaches could evolve as a TcB surrogate.

An important issue reported in clinical TcB devices is both increased error and a systematic overestimation bias in black African neonates (LOA of 6.7 to -0.65 mg/dL with a bias of 3.04 mg/dL) [95]. TcB nomograms constructed using only black African neonates [96] have been shown to address these issues, indicating these problems may arise from skewed racial composition in enrollment of subjects during construction of the TcB regression models. Enrollment in this pilot study was nearly even between those of African-origin and White infants in an attempt to ensure enrollment biases minimally contribute to model construction. While the overall bias of this study is slightly negative, these pilot results require a more robust statistical assessment of bilirubin value error and racial bias would require a larger scale study. It is worthwhile noting the results from this

pilot study do not indicate either increased error of the over-estimation bias previously seen using TcB for black and African infants.

The fundamentally unique approach used in this study lies in the extraction of multiple individual spectral and spatial offset ROIs from filtered RGB images of spatially-offset diffuse reflectance. While clinical approaches to TcB measure diffuse reflectance in up to two different fixed spatial offset channels using between 2 and 5 wavelength channels to create a model for bilirubin estimation [67], the approach described here utilizes 9 uniquely optimized spatial ROIs across 3 different wavelength channels to inform a GLM [76]. Alternatively, the collection of multiple color-calibrated photographs of neonatal skin [72] have also been reported for accurate estimation of bilirubin levels (LOA of 3.6 to -3.6 mg/dL with 0.0 mg/dL bias) using algorithms not directly inspired by clinical TcB. In addition, measurement of neonatal skin using a mobile-phone camera dermatoscope has also reported the ability to correlate with TSB in Caucasian infants ($R^2=0.81$) [12]. It is possible that the differences in measurement techniques may produce different TSB estimation characteristics; although, further studies would be necessary. An important limitation of this pilot study is the relatively low number of enrolled infants with respect to the naturally skewed, non-normal, nature of newborn TSB distributions. A larger scale study with increased enrollment of infants with elevated TSB levels would be beneficial and reduce the need for resampling and large scale cross-validation to produce a generalized model.

Selection of an appropriate acquisition time that would allow proper exposure of the spatial decay of spatially offset diffuse reflectance across the RGB color channels

represented a challenge for measurement configuration. The approach reported here requires configuring the camera hardware to collect the raw, uncompressed, 16-bit output of the detector array, as opposed to a JPEG compression, in order to retain the ability to perform absolute quantification of reflectance and preserve the available dynamic range of the detector. The more than 2-fold difference in the red channel to blue channel reflectance coupled with the requirement for large, uncompressed raw image data motivated the selection of a single exposure time which served as a compromise. Thus, this allowed the collection of maximal signals in the blue channel while still retaining a limited range of un-saturated reflectance in the red channel. Monte-Carlo models of reflectance in neonatal skin were used to investigate the benefit of altering source-detector offset in order to increase blue channel reflectance. Alternative strategies such as the collection of multiple raw images at different exposure times for high-dynamic range compression represents a promising future strategy which may improve the spatial range of unsaturated data available to place ROIs. While this may improve the TSB prediction model, collection of such large file size datasets was not feasible in this study.

The wide variety of mobile device models presents a challenge for many techniques developed atop mobile phone camera platforms. The technique we described would require the re-design of the adapter module that prioritized a similar field-of-view and illumination spatial-offset. Additional calibration of spectral throughput would also likely be necessary and could be performed using the same calibration measurements performed in this study.

Conclusion

The availability, accuracy and cost of current TcB devices remains an obstacle for their adoption within low-resource settings and LMICs as part of standard practice. The results presented here show that a mobile phone camera based TcB device using a simple, passive, adaptor and unique algorithm for extraction of multiple spatial and spectral ROIs from images of spatially-offset reflectance holds potential for estimating TSB, however additional developments will be necessary before the technique may prove valuable in LMIC settings.

4. FEASIBILITY STUDY OF MOBILE PHONE-BASED TcB APPROACH TO IMPROVING THE MANAGEMENT OF NEONATAL JAUNDICE

Abstract

Screening newborns for neonatal jaundice with a transcutaneous bilirubinometer (TcB) is a common practice in high-income countries. However in low- and-middle-income countries (LMIC), accessibility to TcB is limited due to a lack of resources. Developing a mobile phone-based approach may help broaden screening opportunities within LMIC. In this study, we further validated a mobile phone-based approach and method for TcB in a 91 patient multi-site pilot study. Included is a calibration method for a mobile phone-based system variance by combining datasets collected with multiple phones from multiple sites. Measures of reflectance were extracted from multiple optimized spatial-offset regions of interest (ROIs) and a linear model was developed and cross-validated. This resulted in a correlation between total serum bilirubin and mobile-phone TcB estimated bilirubin with $R^2 = .28$ and Bland-Altman limits of agreement of 9.2 mg/dL to -9.3 mg/dL. These results indicate that an adapter-based smartphone can be modified to measure neonatal bilirubin values and provide a novel, affordable tool for neonatal jaundice screening in low-resource settings.

Introduction

During the first week of a neonate's life, it is very common to develop a condition known as neonatal jaundice (NNJ). This is a condition that is characterized by the

yellowish discoloration of the skin and an elevation of serum bilirubin levels [54]. Extreme hyperbilirubinemia (EHB) over an extended period of time can lead to severe neurosensory deficit, kernicterus (permanent brain damage) and even death if left untreated [44]. Neonatal mortality due to EHB is 172 times higher per 10,000 births in low- and middle-income countries (LMIC) than high income countries (HIC) [55]. This can be attributed to the improvement of systematic approaches in screening, diagnosing, monitoring and treatment in HIC versus LMICs. High volumes of home births and inconsistent access to healthcare facilities prevent the gold standard total serum bilirubin (TSB) testing which is routinely conducted in HICs [56], [58], [59]. Therefore, visual examination of the skin through blanching is the primary method for evaluation in LMICs despite its limited accuracy and predictive power of EHB in comparison to TSB [59]–[61]. Many research groups have shown the strength of low-cost point of care blood assessments to improving EHB outcomes in LMICs [62], [64], [97]. However, these approaches are invasive techniques that require consumables, which makes them less preferable when compared to noninvasive approaches.

Transcutaneous Bilirubinometry (TcB) is a noninvasive optical reflectance screening technique that measures bilirubin levels using absorption peaks at 460 nm, another absorption peak above 500 nm to regulate optical difference in neonatal skin due to perfusion, pigmentation and scattering, and utilizes the detection of these absorption peaks at two specific spatial offsets [66], [67]. TcB devices have become a crucial component for systematic improvement for screening neonates at risk of EHB in HIC [68], [94]. This systemic application has improved the timeliness of treatment and, more

importantly, reduced instances of Chronic Bilirubin Encephalopathy (CBE) and EHB-related deaths in HIC [55], [71].

Over the last 20 years, TcB has become an important element in a systematic approach for screening a newborn's risk for EHB in HIC [68], [69]. As a result, appropriate treatments are administered in a timely fashion, and instances of CBE and EHB-related deaths are extremely rare in industrialized countries such as the United States [55], [71]. Expanded adoption of TcB in LMIC has been proposed, but the cost of currently available TcB devices remains an obstacle. As a result, development of low-cost and mobile phone-based approaches to estimate serum bilirubin levels have been proposed [12], [51], [72]. In particular, a mobile phone-based platform offers strong potential for integration with communications networks for coordination of care, healthcare data management and real-time patient monitoring [73]–[75]. With an appropriate use of spectral filters and unique imaging techniques, LMICs can take advantage of widely accessible mobile phones to lower morbidity rates due to EHB.

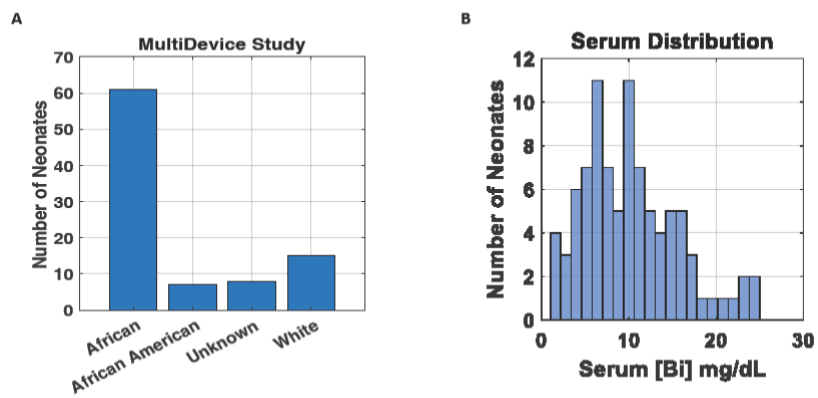
The development of a mobile phone-based TcB device has been previously reported with a smaller feasibility study. Here, we describe a continued feasibility study conducted in additional LMIC settings. The approach mimics clinical TcB by directly measuring spatially-offset diffuse reflectance in direct contact with the infant's skin. This feasibility study was performed across two sites in Tanzania and Nigeria in order to further validate the use of this mobile phone-based TcB device, as well as the development of a generalized linear model using multiple spatial offset regions of interest

(ROIs) across three red, green and blue (RGB) reflectance channels. To date, no mobile phone TcB device has shown feasibility in LMICs.

Materials & Methods

Human Subjects

Measurements were collected utilizing the mobile phone-based TcB device from 91 neonates (30 from Vanderbilt University Medical Center (VUMC) in Nashville, TN, USA; 28 from Aminu Kano Teaching Hospital (AKTH) in Kano, Nigeria; and 33 from Muhimbili National Hospital (MNH) in Dar es Salaam, Tanzania). Healthy infants between 24 and 72 hours postnatal age were considered eligible for this study. Exclusion criteria included infants born with known or estimated gestational age < 32 weeks, weighed under 1500 grams, or prior phototherapy. Each mobile phone measurement was obtained within 30 minutes of a blood sample used to obtain TSB. Written consent was obtained from all parents, and all studies were performed in accordance with the institution's human subjects research approvals (VUMC IRB130471, AKTH EC1390, Muhimbili). All measurements were collected using the smartphone in direct contact with the sternum of the infant. The demographic distributions of the neonates are provided in Figure 4-1A. The distribution of TSB values obtained for all neonates are shown in Figure 4-1B, indicating a right-skewed, non-normal distribution characteristic of newborn TSB, with a majority of values between 1-10 mg/dL, and some infants with elevated values as high as 23.7 mg/dL.



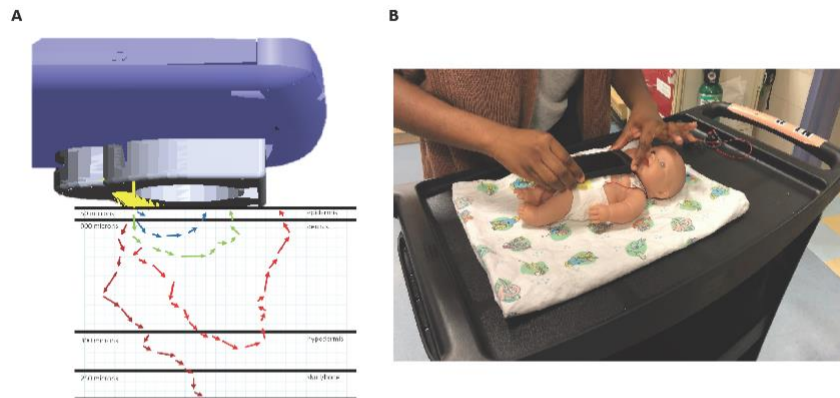
1

Figure 4-1. Study Demographics. (A) Racial Ethnicity of patients enrolled in the study: 61 Africans, 7 African Americans, 15 white and 8 race unknown neonates. (B) Enrolled neonates corresponding serum bilirubin values.

Device Measurements

A custom mobile application was developed in order to configure mobile phone image acquisition, as well as guide users through calibration and clinical measurements. The basic interface of the smartphone application during image capturing is presented in Figure 4-2. Image data is configured to be saved without pre-processing or compression in raw 16-bit format in order to ensure the data could be used for quantitative measurement of reflectance. Camera acquisition parameters were fixed, including focus, exposure time and ISO/gain. Each measurement consisted of acquisition of 3 successive tissue reflectance images with exposure time of 400 ms and ISO of 4500, along with a

paired set of 3 dark background images collected with the LED off. In this study, 3 replicate sets of measurements were collected from each infant to ensure unexpected clinical scenarios such as sudden movements did not reduce enrollment yield.



1

Figure 4-2. Mobile Phone TcB Device

Calibration was performed by measurement of a custom calibration standard consisting of a 25x25x5 (thick) mm High-Density Polyethylene (HDPE) white plastic block housed in a Vero black casing using an identical sequence of reflectance (LED on) and background (LED off) image acquisitions. Paired calibration measurements were collected for each patient enrolled.

Region of Interest (ROI) Based Generalized Linear Model

Optical estimation of bilirubin levels with clinical TcB is typically assessed through the creation of regression models of diffuse reflectance measurements at specific spectral channels and multiple offsets [67]. In our report, we designed an approach which constructs a linear model by selecting unique ROIs with a pattern search algorithm. A data-driven approach was used to train and cross-validate a bounded pattern search algorithm which optimized placement of specific spatial offset channel regions of interest (ROI) for use in a generalized linear model (GLM) to predict TSB.

A bounded pattern search algorithm implemented in the MATLAB optimization toolbox (Mathworks) was used to optimize ROI placement for the linear model [84]. Here, the spatial offset areas are arc-shaped regions of interest (ROI) in each spectral (RGB) image frame defined based on their position, radius and width. Initial conditions for 4 ROIs in the blue channel, 3 ROIs in the green channel and 2 ROIs in the red channel are shown in Figure 4-3A. The pattern search algorithm extracts mean values within the ROIs as the observed variables for a gamma distribution (non-negative constraint) based GLM to predict TSB [85]. The pattern search algorithm aims to iteratively adjust the positions of the ROIs in order to optimize the sum square error of the GLM over a duration of 900 s. After completion of the pattern search, the predicted values of the test set are stored in a table, and the training/testing routine is cross-validated over 3,000 iterations, resulting in 21,000 estimates (roughly 550 per patient). The median predicted value for each set of predictions for an individual patient is then determined to be the final predicted patient value. A correlation plot for predicted bilirubin values compared to

TSB and a Bland-Altman plot were generated to report model performance, bias and limits of agreement. In addition, the final ROI parameters were calculated as the mean positions across all cross-validations.

Multi-Site Calibration Method

OD devices customarily have to be calibrated for system and intra-device variance in measured signal for uniform data comparison. In this study, a two stage calibration approach was used to account for inner-device patient measurement differences and intra-device differences as seen in Figure 4-4. Inner phone calibration was developed by creating a ratio between the corresponding device calibration and calibration measurements made at the point of each patient measurement. This creates a scaling affect which is then applied to the patient sternum images which is labeled as the inner phone calibration. The second stage calibration is developed by creating a ratio between corresponding devices calibration against device 2's calibration. Device 2 was used to scale the other devices to its calibration. This was known as the multi-phone calibration, which is applied to the patient sternum images after inner device calibration.

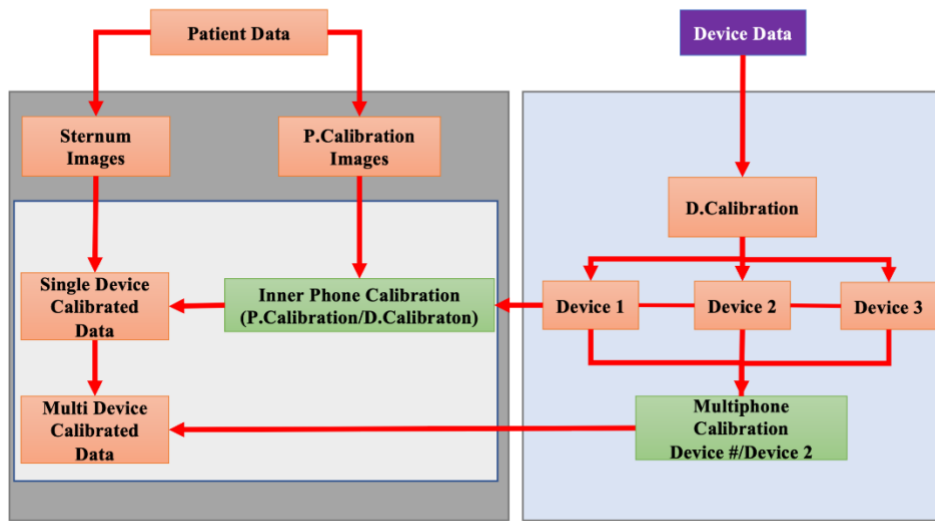


Figure 4-3. Calibration Method for Aggregation of the Data.

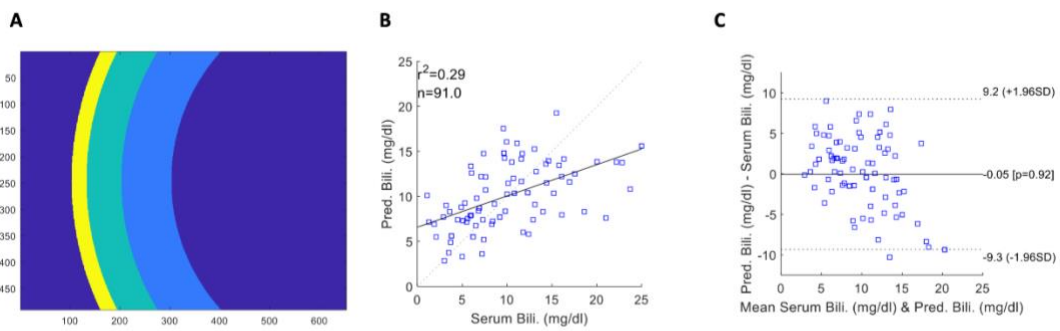


Figure 4-4. Linear Regression Statistics. (A) ROI position. (B) Correlation of Device predictive [Bi] vs TSB [Bi] n=91. (C) Bland Altman of Device Bias and Confidence.

Results

Bilirubin levels were evaluated in a continued pilot study conducted at Vanderbilt University Medical Hospital (VUMC), Aminu Kano Teaching Hospital (AKTH) and Muhimbili National Hospital. Figure 4-1A represents a demographic breakdown of the 91 neonates that participated in this study. There are 61 African, 7 African American, 15 Caucasian and 8 race unclassified neonates. TSB and mobile phone-based TcB measurements were collected from each patient. The measured bilirubin TSB levels complemented the clinical bilirubin range from 0-25 mg/dL, with the majority ranging between 5 and 15 mg/dL. Figure 4-3B shows a correlation for the predicted TSB levels from the mobile phone-based TcB device with an R^2 value of .28. The Bland-Altman plot in Figure 4-3C shows a mean difference of -0.05 mg/dL between the mobile phone-based TcB device and TSB measurements, and 95% Limits of Agreement (LOA) are 9.2 mg/dL to -9.3 mg/dL (range between the upper and lower limits of LOA equal to 18.5 mg/dL).

Discussion

Severe NNJ contributes to up to 5-14% of neonatal deaths or causes varying degrees of neurological abnormalities in neonates [60]. Addressing the burden of severe NNJ in LMIC is complex due to challenges in limitations in maternal education, adoption of universal practices for newborn screening and expansion of availability of treatments [88]. A mobile phone-based approach to bilirubin screening could reduce the global burden of NNJ by utilizing the mobile phone's vast accessibility even in low-resource and rural areas in LMIC and has substantial potential to improve screening practices, if

effective [89]. In addition, the mobile phone offers the ability to expand the coordination of treatment, data tracking and service to neonates needing care in remote areas.

In this study, we report the feasibility of a mobile phone-based approach for TcB measurement that utilizes an optical adapter fitted to a mobile phone case. The adaptor paired with the mobile phone enables collection of spatially resolved images of diffuse reflectance. A previously developed method for extracting multiple spatial and spectral ROI reflectance channels within the RGB image data was used to estimate bilirubin levels in neonates. With 91 enrolled neonates in the study, this mobile phone-based approach reports bilirubin estimation 9.2 to -9.3 mg/dL, with a bias of -0.05 mg/dL (Figure 4-3C). These results are poor in comparison to our previously reported results with 6.4 to -7.0 mg/dL, with a bias of -0.28 mg/dL. This suggests limitations with the approach of combining data into a larger study.

The calibration used in this study is a technique of inner-calibration and intra-calibration. The inner calibration is designed to remove variance between patient to patient measurements. This calibration produces a scaling factor in which the data scales up or down in intensity. The intra-calibration is meant to do the same things but with differences due to device variation.

These poor results could potentially arise from variance between collection of images with this device. The device measurements should be taken flat and flush against the neonate's skin. There are qualitative differences between a portion of the patient data collected that suggests a need to better standardize across patient measurements that cannot be captured in calibration measurements. Calibration images did not reflect the

differences that were seen in the sternum images. Future alterations to this approach need to include ways to normalize measurements between users.

Alternative issues could be due to the saturation of the dynamic range of the images. The saturation of data may distort the model's ability to select appropriately spatially offset information from the image. Future modifications to this approach should include techniques that increase the dynamic space of the images used in the model construction. Strategies include acquiring multiple images at different exposure times and using them to create a high dynamic range image.

The availability, accuracy and cost of current TcB devices remain an obstacle for their adoption within low-resource settings and LMICs as part of standard practice. The results presented here show that a mobile phone-based TcB device using a simple optical adaptor and unique algorithm for extraction of multiple spatial and spectral ROIs from images of spatially-offset reflectance needs refinement if it is to prove valuable in LMIC settings.

5. IN SILICO ANALYSIS OF BILIRUBIN QUANTIFICATION USING SPATIALLY RESOLVED DIFFUSE REFLECTANCE WITH A MOBILE PHONE CAMERA

Abstract

Hyperbilirubinemia is a neonatal condition that can lead to the development of brain damage or even death if left untreated. Health disparities exist in the management of hyperbilirubinemia in low- and middle-income countries, partly due to limited accessibility and substandard accuracy of screening approaches. There is increasing interest in utilizing mobile phone platforms for diagnostic approaches in order to increase screening accessibility. Recently, we reported the development of a 2d spatial diffuse reflectance technique for measuring bilirubin levels in neonates diagnosed with jaundice. This technique reduces the dimensionality of a 2d image space by reducing dimensions into spectral and spatial channels for a region of interest through pattern search predictive model construction. While feasibility of the mobile phone device was proven, limited understanding from the selected region of interest spectral and spatial channels persists. In this study, we perform a phantom study to explore the impact that increased sample chromophore dimensional variability has on the predictive model correlation. Phantoms were created to simulate the variability of blood, bilirubin and melanin, and then imaged with a mobile phone-based TcB device. Mean intensities of systematic selection regions of interest based on spatial and spectral images were used as prediction variables for multiple linear regression model construction. The results of this study suggest that 2d

spatially resolved diffuse reflectance models benefit the most from unique spatial and spectral regions of interest.

Introduction

Diffuse reflectance (DR) is a commonly used technique for acquiring transcutaneous measurements of physiological parameters through the skin, including blood oxygenation, heart rate, bilirubin levels and hydration [3], [22], [35], [47], [98]. Spatially-resolved observations have long been understood to enable recovery of optical properties in tissues, improve estimation accuracy and improve depth localization in reflectance measurements from tissues [99]–[103]. Due to the complex makeup of the skin, transcutaneous devices, such as the bilirubinometers and also more recent commercially available wearable sensors, incorporate multiple spatial or spectral channels detection channels to extract estimates of optical biomarkers [29], [67], [104]. Signals collected at longer source-detector offsets probe information that has interacted with a volume of tissue which, on average, extends deeper into the tissue [17], [18]. However, it is well understood that diffuse optical measurements are the product of interactions with different layers of the skin, each with varying levels of scattering and chromophore complexity that contributes to total variability in the collected light signals and different nonlinear patterns of reflectance [23]–[25].

DR measurements used to create quantitative estimate variables, such as serum bilirubin or blood oxygenation, rely on the construction of analytical models, which can range from simple linear regression to adaptive neural-networks [20], [105]. Inverse

techniques that aim to solve directly for the theoretical composition of chromophores of interest in the dermis, such as bilirubin, deoxygenated/oxygenated hemoglobin and melanin, prove challenging because of the fundamentally ill-posed nature of the mathematical solution [106]. Data-driven, machine learning-based techniques can require large data sets and careful cross validation, but are ultimately very promising techniques that are excellent solutions in many circumstances [107]–[111]. In diffuse optical detection schemes with multiple spatial channels, multivariate linear regression is a simple technique well-suited for model construction [112], [113]. An important factor in performance of multivariate regression is that each additional input variable with incremental differences in collinearity with prior variables will improve model construction [114], [115]. In the case of spatially resolved diffuse reflectance measurements, the unique relative contributions from optical chromophores across tissues layers can provide a benefit in prediction. While prior spatially resolved diffuse reflectance techniques were primarily based on discrete spatial detection channels defined by fiber optics or photodiodes, an alternative is to use a 2d camera and define unique spatial channels within the image itself [116]–[119].

Transcutaneous Bilirubinometry (TcB) is an important clinical technique for screening newborns for hyperbilirubinemia. It is more objective than simple techniques such as icterometry, and it does not require the laboratory facilities and consumables necessary for gold standard total serum bilirubin (TSB) testing [120]. Severe outcomes due to hyperbilirubinemia including neurosensory deficit and even death are primarily limited to low- and middle-income countries (LMIC) due a variety of systemic and

epidemiological factors; however, one factor is the limited adoption of bilirubin screening techniques [68], [88]. A number of groups have pursued the development of mobile phone camera-based techniques to estimate bilirubin levels with varying degrees of success. Our group has previously reported the feasibility of a mobile phone camera-based approach that seeks to perform a modified estimation of TcB. This is accomplished through the extraction of 9 unique spatially resolved detection channels across 3 spectral wavelength bands extracted from 2d spatially resolved DR images from neonatal skin for construction of a linear regression model against TSB [104]. In contrast, widely used clinical bilirubinometers including the Draeger JM-103 and Philips Bilicheck, utilizes between 2-6 spectral channels, but no more than 2 spatial channels [47], [121]. However, decreased accuracy and bias reported while using these devices on Black African neonates indicate current approaches for estimation of bilirubin values retain residual error in their analytical models that do not fully account for pigmentation-dependent effects on DR signals [96].

In this manuscript, we perform a fundamental *in silico* investigation of the fundamental performance of multivariate linear regression models constructed using 2d spatially resolved diffuse reflectance images collected from a mobile phone-based TcB device. This was accomplished by constructing regression models for a chromophore mimicking bilirubin within from measurements obtained from two layer skin mimicking phantoms. The compositional complexity of the phantom was expanded to include confounding factors mimicking blood and superficial melanin. Ultimately, expanding the

number of spatially resolved channels beyond 2 improves the performance of the model and suggests promise for future transcutaneous measurements.

Materials & Methods

The overall approach in this manuscript involves the fabrication of skin mimicking optical phantoms with varying degrees of compositional complexity, followed by creation of multivariate linear regression models for a bilirubin analog that utilizes an increasing number of spatially resolved DR measurement channels, as in shown in Figure 5-1A-D.

Tissue Optical Phantoms

Tissue phantoms are engineered with reliable composition and structure and they are widely used for analysis and characterization of optical techniques, including transcutaneous measurements [122]. In this study, phantom composition includes chromophores that mimic bilirubin, hemoglobin and melanin present in the skin.

Polydimethylsiloxane (PDMS) (Sylgard 184 Silicone Elastomer DOW/Corning) optical phantoms with embedded scattering and absorptive elements were fabricated following the protocol shown in Figure 5-1A [123]. The selection of PDMS and the specific chromophores was based on achieving stable shelf-life and producing optical properties that mimicked tissue chromophores. Yellow dye 6 (Sigma Aldrich, Co.) was selected as a shelf-stable analog of bilirubin as they both exhibit an absorption maxima near 470 nm [124]. Dissolved instant grind coffee crystals (Folgers Classic Roast®

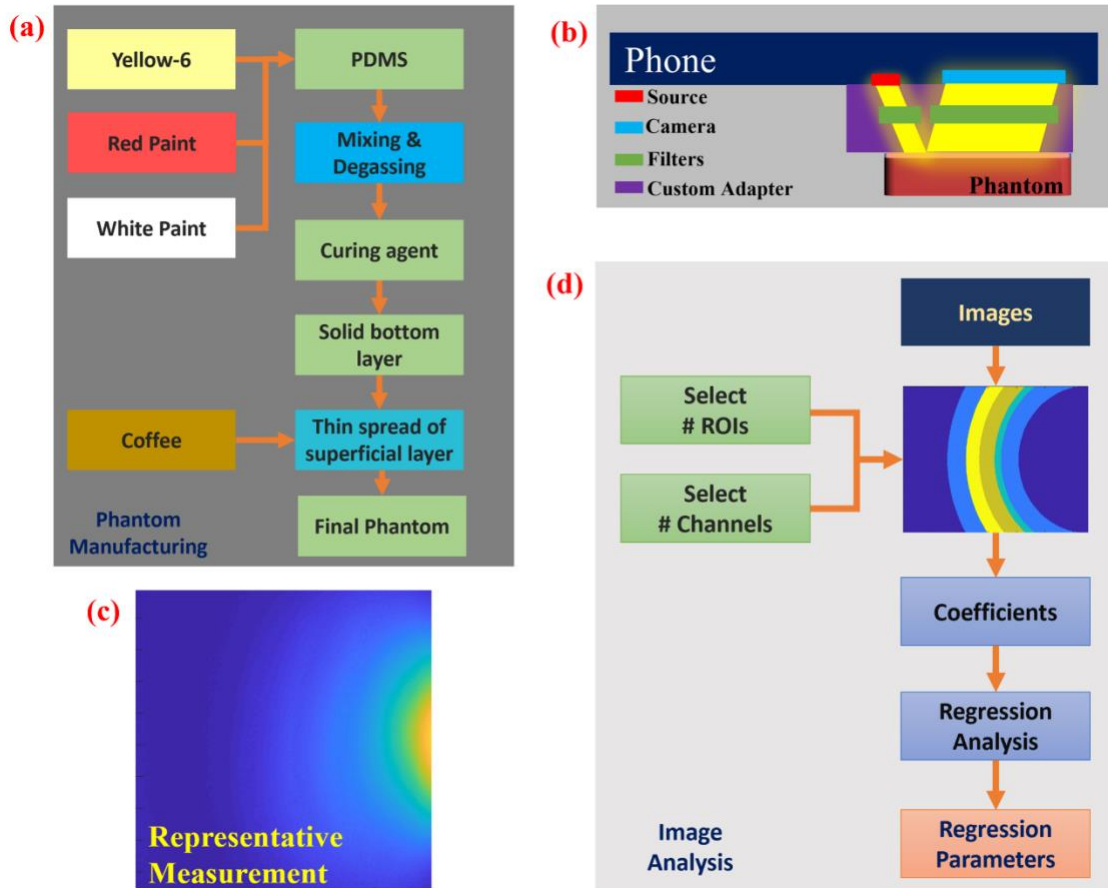


Figure 5-1. Phantom Fabrication and Image Analysis. (A) Fabrication of two layer skin mimicking PDMS optical phantoms. (B) Imaging of phantoms with the mobile phone-based TcB device (a modeled representation of the device and setup. Not to scale). (C) Single channel representative image from a phantom. (D) Image analysis and regression model construction procedure.

Instant Coffee Crystals) were selected as stable analogs of melanin [125]. Red paint served as a chromophore with an absorption maxima near 550 nm to simulate hemoglobin. White paint 2.0 (Culture Hustle USA) was incorporated into the PDMS to mimic scattering. Yellow dye 6, red paint and white paint were added to a single mixture of PDMS, which after curing, resulted in a homogeneous single layer phantom that mimics the vascularized dermal layer of the skin in which bilirubin and hemoglobin reside. A second layer was cured on top of the dermal layer with coffee and white paint to simulate the epidermal layer. The dermal layers were cast in individual 25x25x1.7 mm custom 3d printed molds. The epidermal layer was cast on top of the dermal layer with a single 60 micron thick adhesive tape (Scotch® Magic™ Tape) as the cast to replicate the thickness of neonatal skin [126]. The mixtures were degassed for 30 minutes and placed into an oven at 80°C for 4 hours. Phantoms layers are fabricated by adding scattering and varying concentrations of absorbers to the volumes of PDMS(10 ml) used. All phantom layers maintained the same concentration of white paint at 40 μ l per volume of PDMS. Three separate concentrations of yellow dye 6 (40/50/60 μ l per volume of PDMS), red paint (50/60/70 μ l per volume of PDMS) and coffee (25/100 μ l per volume of PDMS) were used to create a 3x3x2 phantom table with each slice of the table representing a separate melanin concentration, as shown in Figure 5-2. Figure 5-1A shows the overall process of phantom fabrication.

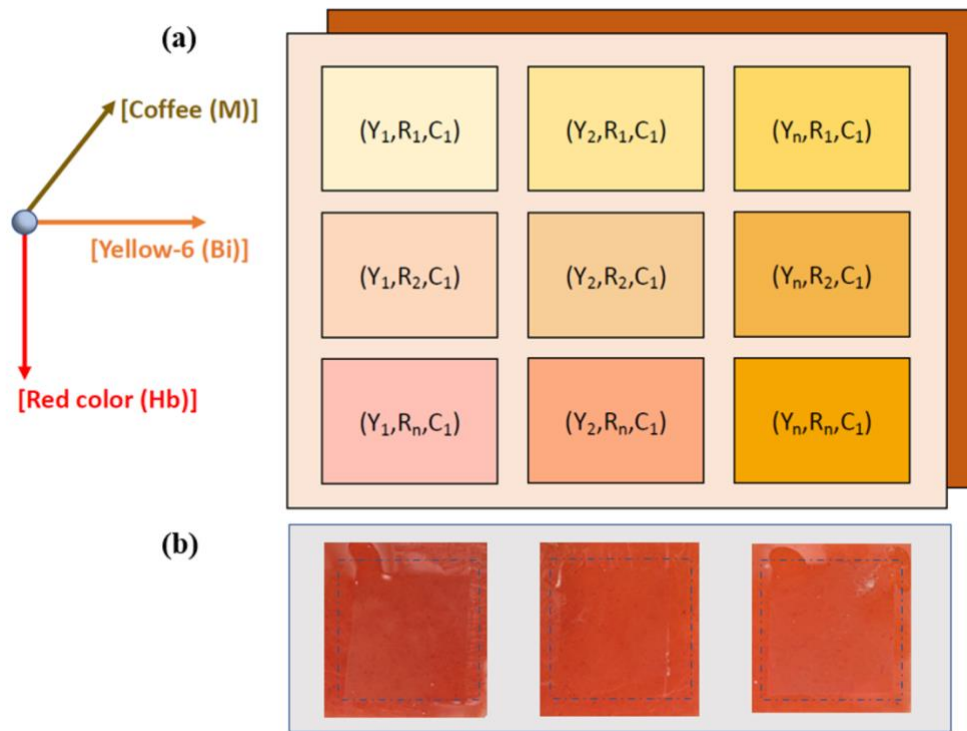


Figure 5-2. Phantom Chromophore Variability Matrix. (A) Depicts the compositional makeup of optical phantoms where each slice represents different melanin concentrations. (B) Representative picture of the phantoms where superficial melanin layer is shown with dashed border.

Mobile Phone TcB Measurements

Mobile phone reflectance measurements of the phantoms were obtained using the on board camera and LED flash of a One Plus 3003A Android mobile phone fit with an optical adapter [104]. Measurements of phantoms were collected in triplicate, with fixed focus and sensitivity. Exposure time was set to 400 ms. Background measurements taken with illumination flash off and the camera aperture blocked, and then subtracted from sample images to produce measured DR. A representative setup for mobile phone image acquisition and a representative image from one of the three spectral channels (blue, green, red) obtained from a phantom is portrayed in Figure 5-1B-C. All images are 900 H x 1200 W pixels in size.

Regression Model Construction

Input variables for construction of multivariate regression models were extracted from the average DR from within ROIs placed on the averaged image. ROIs were defined as arcs with inner and outer radii located at a position outside the image-space corresponding to the illumination spot (Figure 5-3). Multivariate regression models were constructed for prediction of yellow dye 6 concentration within the phantom, and regression model statistics (R^2 , significance (*p-value*)) were used to evaluate model performance, as shown in Figure 5-1D.

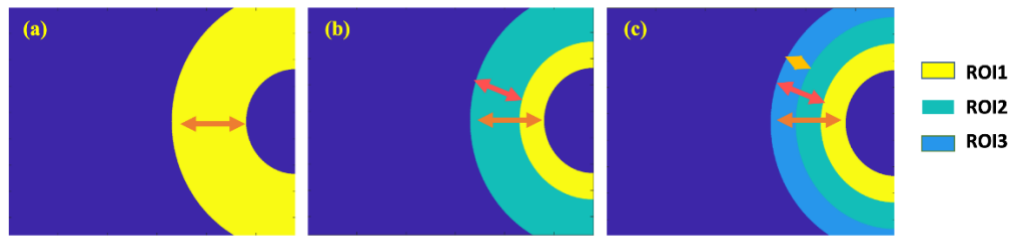


Figure 5-3. Region of Interest (ROI) Positioning. (A) Placement of a single ROI represented by a yellow arc. (B) The placement of two ROIs is represented by a yellow arc and a cyan arc. (C) The placement of three ROIs is represented by a yellow, green, and cyan arc.

Results

A mobile phone-based TcB device was utilized to evaluate the performance of multivariate linear regression models based on different numbers of spatial and spectral input variables extracted from 2d spatially resolved images of the DR from a spatially offset point-source. Regression models were created using different subsets of phantoms in order to relate model performance with the complexity of phantom composition. Figure 5-2A illustrates this 3x3x2 phantom matrix where each sheet of phantoms represents a different coffee concentration; mimicking low- and high-skin pigmentation groups. Within each pigmentation mimicking phantom subset, each row of phantoms contains an increasing concentration of yellow dye 6 and each column of phantoms varies red dye concentration. Regression models were constructed from phantom subsets with

progressively increasing complexity in both composition and input variable dimension (Figures 5-4-8). When an additional ROI was added in a given spectral channel, the larger ROI was subdivided as depicted in Figure 5-3A-C to ensure mean spatial offset and signal intensities were unaffected, in an effort to focus analysis on the effect an increasing the number of input variables in multivariate model construction.

Figure 5-4A-B represents the univariate regression models produced for a subset of phantoms with fixed red dye and coffee concentrations (i.e. a single row of phantoms as depicted in Figure 5-2A with only 1 blue ROI selected). In each model, there is a positive correlation between the predicted yellow dye concentration and actual experimental calculated concentration. Figure 5-4 confirms the expected result that a single ROI can predict yellow-dye concentration with varying levels of strength ($0.43 < R^2 < 0.95$) in simplified phantom subsets where there is only a single dimension of variability which corresponds to regression output.

The strength of the univariate (1 blue channel ROI) regression also varies with ROI placement (Figure 5-5), which is expected, since the decrease in overall signal levels reduces predictive performance of the measurements. Figure 5-5A illustrates the two extreme positions for the 15 uniformly spaced ROIs, each translated by 50 pixels in the image space. Figure 5-5B demonstrates how the change of spatial offset incrementally impacts the linear regression model (low coffee concentration (Figure 5-4A)) as the ROI position changes. Here, model performance deteriorates as seen by a decrease in R^2 (Figure 5-5C) and an increase in p-value (Figure 5-5D) with increasing ROI position and

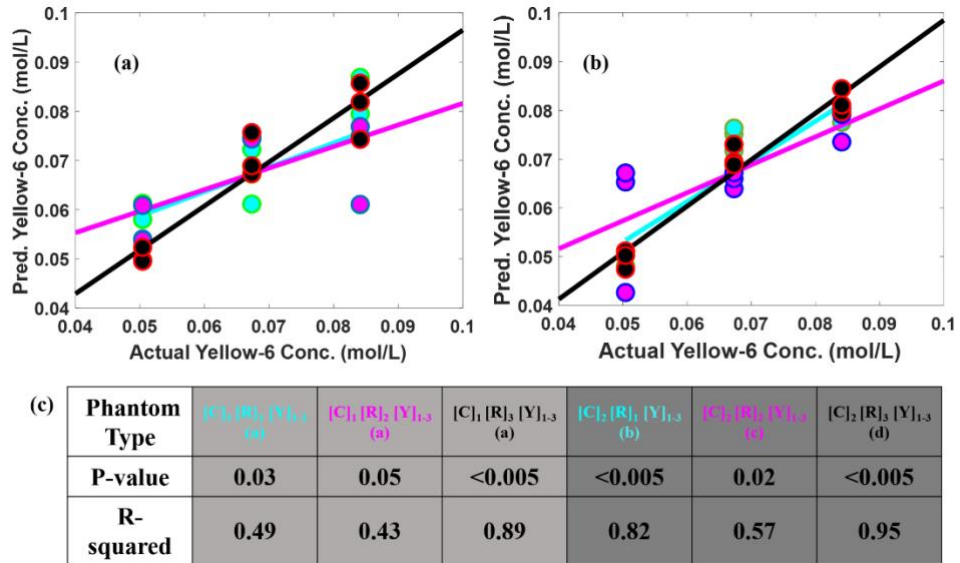


Figure 5-4. Simple univariate regression model for yellow dye 6 with 1 blue channel ROI where concentration of coffee and red dye was fixed. (A) Regression models for 3 unique red dye concentrations and low coffee concentration based phantoms concentration used for model construction. (B) Regression models for 3 sets of varied high coffee concentration based phantoms used for model construction. (C) R^2 and P values for the linear regression models created in Figure 5-4A-B. Here, cyan represents the phantoms with the lowest concentration of yellow dye 6, magenta for the middle concentration of yellow dye 6 and black for the highest concentration of yellow dye 6.

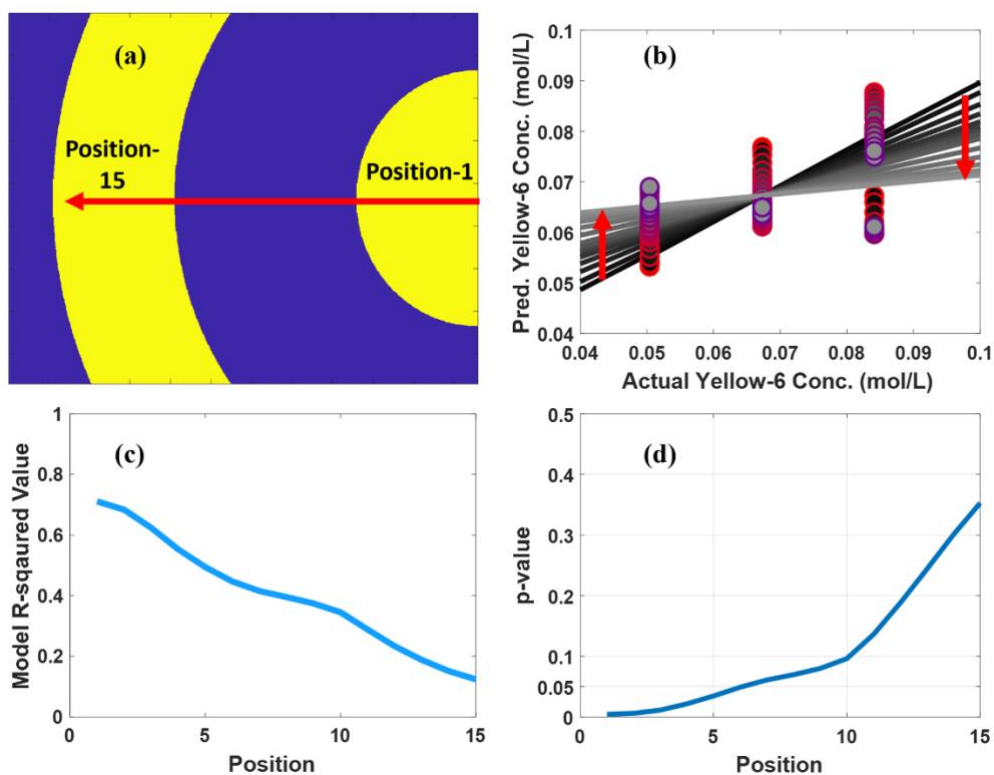


Figure 5-5. A simple univariate regression model for yellow dye 6 varies with ROI placement position. Linear regression models were constructed with 1 blue channel ROI with a fixed concentration of coffee and red dye. (A) Arc position placement. Arc was translated from position-1 to position-15 in uniform increments. (B) Models were created from 15 different Arc positions. The darkest shade of black represents the position-1 regression line, lightest shade represents position-15. The red arrows show the movement of the regression line from the initial position to the final position. (C) P-values for each linear regression model created in Figure 5-5B. (D) R^2 values for each linear regression model created in Figure 5-5B.

spatial offset. In the context of regression, these results indicate that ROI position is an important factor in model performance, a concept well understood spatially offset diffuse reflectance, and not surprisingly, also supported here.

When the subset of phantoms used for regression model construction was expanded to a more complex scenario that includes variation across three levels of red dye concentration, while coffee concentration remained fixed, regression becomes more challenging (Figure 5-6). Univariate regression models constructed using 1 blue channel ROI for both the high and low coffee phantoms (Figure 5-6A) indicate a deterioration in model performance in comparison with identical models from Figure 5-4. Regression performance deteriorates from a range of ($0.43 < R^2 < 0.89$) to ($R^2 = 0.17$) for low coffee phantoms, and ($0.57 < R^2 < 0.95$) to ($R^2 = 0.56$) for high coffee phantoms. Here, when the dimension of the regression model is expanded to include 2 input variables either both in the blue channel (Figure 5-6B) or 1 blue and 1 green channels (Figure 5-6C), only modest improvement is observed.

Inclusion of all phantoms, including variations in red dye and coffee, represented a final expansion in the complexity of phantom composition for regression model construction. Regression models were constructed with 2 ROIs (1 blue and 1 green spectral channel (Figure 5-7A)), 3 ROIs (1 blue, 1 green and 1 red spectral channel (Figure 5-7B)), and 6 ROIs (2 blue, 2 green and 2 red spectral channels (Figure 5-7C)). Regression statistics for these models as shown in Figure 5-7D indicate comparable performance between 2 and 3 regression input variables ($R^2 = 0.26, 0.27$), but a large improvement when a multi-variate regression with 6 input variables is constructed

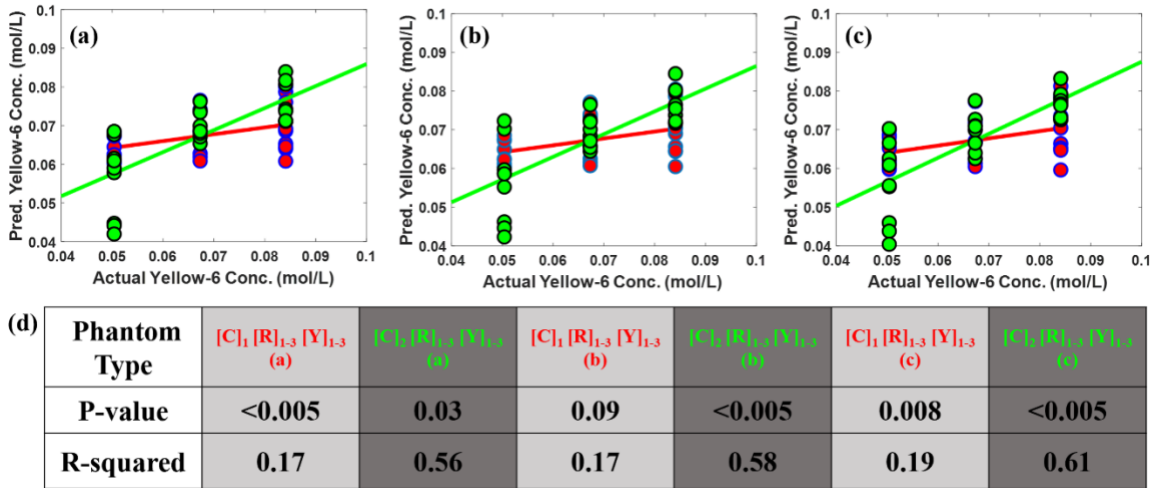
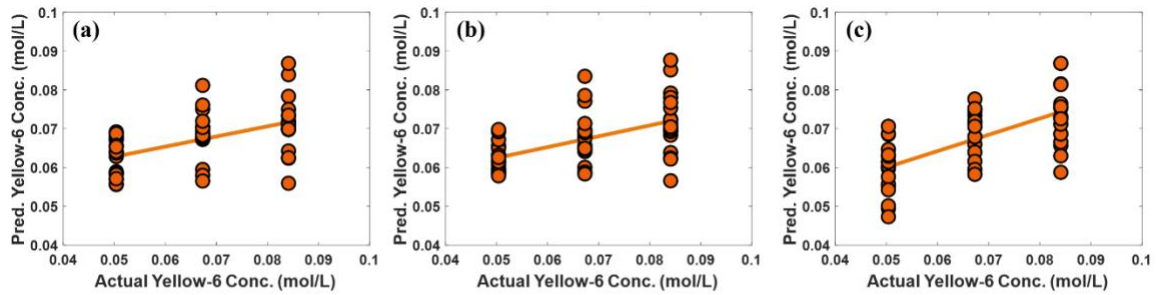


Figure 5-6. Linear regression for yellow dye 6 with varying red dye and fixed coffee concentration with less than two ROIs (A) 1 blue channel ROI; (B) 2 blue channel ROIs; and (C) 1 blue and 1 green channel ROI. (D) P-values and R^2 values for each linear regression model created in Figure 5-6A-B. Red indicates the phantoms with lower coffee concentrations and green indicates the phantoms with higher coffee concentrations.



(d)

Phantom Type	$[C]_{1,2} [R]_{1,3} [V]_{1,3}$ (a)	$[C]_{1,2} [R]_{1,3} [V]_{1,3}$ (b)	$[C]_{1,2} [R]_{1,3} [V]_{1,3}$ (c)
P-value	<0.005	<0.005	<0.005
R-squared	0.26	0.27	0.42

Figure 5-7. Linear regression models for yellow dye 6 with varying concentration of red dye and coffee with two to six ROIs. (A) 1 blue and 1 green channel ROI; (B) 1 blue, 1 green and 1 red channel ROI; and (C) 2 blue, 2 green and 2 red channel ROIs. (D) P and R^2 values for each linear regression model created in Figure 5-7A-C. Orange indicates the regression line created from all phantoms.

($R^2=0.42$), indicating the benefit that expanding the number of spectral/spatial model inputs has on construction of regression models for yellow dye 6.

A multivariate regression model with 6 input variables can consist of a variety of unique combinations of spectral and spatial input variables extracted from ROIs within the 2d spatially resolved DR image. Figure 5-8 depicts the linear regression models constructed with 2 blue, 2 green and 2 red ROIs (Figure 5-8A, D); 3 blue, 2 green and 1 red ROIs (Figure 5-8B, E); and 2 blue, 3 green and 1 red channel ROIs (Figure 5-8C, E). The position dependence of spatial channel ROIs demonstrated in Figure 5-5 remains with 6 input variables. Regression models are shown in Figure 5-8(A-C) were created using ROIs corresponding to the positions shown in Figure 5-3 and indicate a slight improvement in R^2 when using a greater number of blue channel regression input variables in comparison with green channel input variables. Regression models shown in Figure 8D-E were created with ROIs translated 100 pixels farther away from the illumination point in comparison with Figure 8A-C and the degradation in model performance further supports the importance of ROI position in multivariate regression model performance.

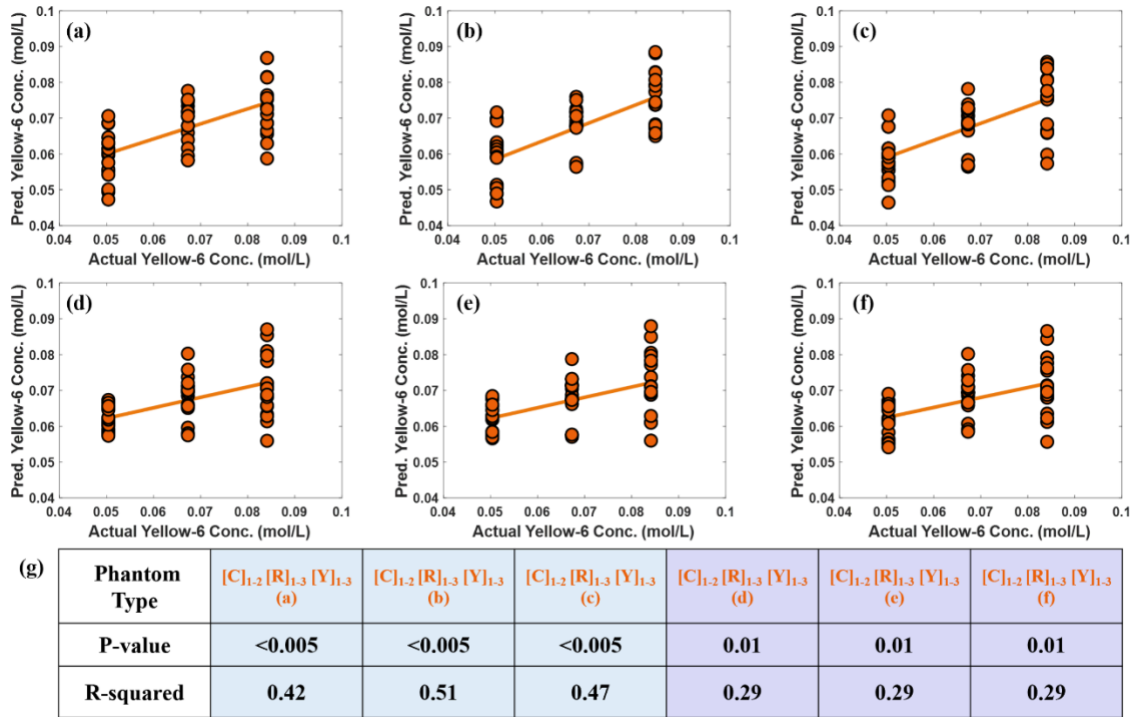


Figure 5-8. Linear regression models for yellow dye 6 with varying concentration of red dye and coffee with six ROIs. (A) 2 blue, 2 green and 2 red channel ROIs; (B) 3 blue, 2 green and 1 red channel ROIs; and (C) 2 blue, 3 green and 1 red channel ROIs. (D-F) represent models respective to Figure 5-8A-C, but with arc placements moved away by 100 pixels from the source. (F) P and R^2 values for each linear regression model created in Figure 5-8A-F.

Discussion

The burden of extreme hyperbilirubinemia in LMIC is multi-factorial, however low-levels of adoption in universal neonatal screening exists in part due to the limited accessibility of techniques capable of providing objective estimates of serum bilirubin levels [43], [46]. Moreover, studies have documented that clinical TcB devices widely used in high income countries are exhibit overestimation bias and higher measurement variability in Black African neonates[1], [2]. Mobile phone-based TcB approaches represent promising techniques for addressing limitations in the screening of bilirubin levels in LMICs [51], [88], [127]. The authors recently reported a mobile phone-based TcB approach [104] that is unique in that it collects filtered RGB images of trans-cutaneous diffuse reflectance from a point illumination. Multi-variate regression models for serum bilirubin were constructed using input variables obtained from six different spatial offset ROIs, however data-driven model construction was limited due to a skewed enrollment of infants with serum bilirubin levels between 4 and 10 mg/dL, a lack of objective measures of pigmentation and perfusion. Moreover, ROI placement was determined through an iterative optimization routine, model performance was sensitive to ROI placement. These factors made analytical assessment of multi-variate regression model construction with respect to known optical confounding factors difficult. Here, an empirical study of multi-variate regression model construction was performed in silico using two-layer optical phantoms. An array of optical phantoms was constructed to model depth-dependent differences in the scattering and pigmentation in the skin across a uniform range of chromophores mimicking bilirubin, blood, and melanin. Muti-variate

regression models were created from input variables defined from spatially offset ROI's placed across the three spectral channels, and analyses were performed to evaluate the influence of ROI position and input variable dimension on regression model performance.

Figure 5-4(A-B) confirms the ability of a reflectance measurements extracted from 1 blue channel ROI to be used in the construction of a univariate regression for yellow-dye with all other variation in phantom composition held fixed. Unique regression models are necessary when phantom red-dye and coffee composition are altered, however it is possible to create a significant correlation in each case (Fig 5-4(C)). Moreover, the strength of the uni-variate (1 blue channel ROI) regression also varies with ROI placement (Fig 5-5), which in this data is primarily due to decreasing signal-to-noise with increasing positional offset. It is also understood that different source-detector separation can alter the depth bias of diffuse measurements[3], [4], however in this configuration the univariate model performance using 1 blue channel ROI is best at the nearest arc position. Regression statistics follow similar trends for other spectral channels with varying levels of agreement with known yellow-6 dye concentration ($R^2 < 0.6$), which indicates that future investigation of analysis techniques pays careful attention to ROI placement, and that there exists a multiplicity of possible ROI spatial channels across spectral channels that could be used for model construction.

Construction of regression models for estimation of chromophore concentration becomes more complex as the number of dimensions in which the sample composition is varied increases. Model performance deteriorates between Figure 5-4 and Figure 5-6A

when variation in red-dye is introduced, and model construction is based on 1 input variable. It is notable that the same spatial/spectral channels exhibit substantial differences in R^2 values in phantoms with low coffee concentrations vs high coffee concentrations in Figure 4 and Figure 6. This supports the need for development of models for bilirubin estimation models that utilize more than 2 spatial/spectral channels in low-cost mobile devices. Model performance also deteriorates from Figure 6(c) to Figure 5-7A when variation and red-dye and coffee is present and model construction is based on 2 input variables. However, the increase in input variables from 2 (Fig. 5-7(A-b)) to 6 (Fig. 5-7C, Fig 5-8) serves to compensate and aid model performance. The question of ROI placement across spectral channels remains an important issue, as is seen via the differences in model performance across Figures 5-8(A-E). Ultimately, the findings from this study support prior work in bilirubinometry and indicate the benefit of more 3 input variables for model construction given expected variations in pigmentation and perfusion amongst neonates in need of screening for jaundice. However, detailed specification of ROI placement and model design would require careful construction of an authentic tissue phantom or human subject studies documenting perfusion and pigmentation levels in addition to serum bilirubin values.

While this study does confirm the fundamental ability to construct multivariate regression models for a bilirubin analog in silico using 2d spatially resolved DR with point illumination, further work will be needed to investigate the additional complexity imparted by scattering, and the relative benefit of additional input variables would have on model construction in these scenarios. Multivariate regression fundamentally

improves only when additional input variables exhibit differing degrees of co-linearity [5], [6]. Thus, it will likely be necessary that ROI's are positioned in spectral/spatial channels with sufficient differences in reflectance from the epidermis/dermis to impart additional benefits to regression. In addition, multivariate regression is an inherently data driven approach, so the size of the current phantom study limits the number of model construction input variables before over-fitting becomes a concern. This phantom study consists of a 3x3x2 matrix that only replicates variations in the skin at the most basic level. A larger phantom study with more phantoms, expanded dimension of variability to include scattering and differences in superficial layer thickness would be beneficial. Alternatively, theoretical studies using Monte Carlo modelling offer excellent opportunities for detailed, flexible analysis.

Conclusion

Limitations of accuracy with clinical and mobile phone-based TcB devices remain an obstacle for adoption in LMICs. This limitation could be attributed to proper selection of wavelengths or spatial channels. In this study, we presented an understanding behind spatial and spectral relevancy in 2d spatial diffuse reflectance imaging. This study showed that relative positions of the spatial channel and model parameter selection influence performance of multivariate regression. Further exploration of spatial and spectral evaluation in phantom models may help improve the redesign of the mobile phone-based TcB device for the adoption of this approach in LMICs.

6. PERSPECTIVE AND CONCLUSION

Mobile phone devices have become commonplace in everyday life; thus, making them a viable platform to transform into an OD device to address disparities of screening device accessibility in LMICs. Overall success and demonstrated value for clinical applications has become a main priority for evaluating emerging techniques in this area.

The goal of this dissertation was to develop a novel approach to the management of neonatal jaundice by utilizing the mobile phone. Various research groups have shown conceptual proof for taking bilirubin measurements through the use of a mobile phone. However, questions of statistical rigor persist due to small sample sizes, generalizability of algorithmic approaches and how these techniques held up in LMICs.

In order to demonstrate the feasibility of a mobile phone-based TcB device in LMICs, the first aim of this work was to perform a small pilot study. Our goal was to assess the ability of the mobile phone-based TcB device and to develop a generalizable approach of image region selection for 2d spatially resolved diffuse reflectance. Details regarding the fabrication and justification of design were demonstrated through Monte Carlo modeling. A unique method for evaluating 2d spatially resolved data was developed and used to predict bilirubin values from neonates in this study. We reported a R^2 value of 0.42 and a limit of agreement from +6.4 mg/dL to -7.0 mg/dL from a study of 37 neonates. These results report the feasibility of a mobile phone with a modified adapter that can be utilized to measure neonatal bilirubin values, thus creating a novel tool for neonatal jaundice screening in low-resource settings.

The second aim of this dissertation was to continue to study the feasibility of the mobile phone-based TcB device with a multi-site and multi-device study. Three pilot studies were conducted with three mobile phone-based TcB devices respectively. In order to combine information collected from separate devices, a method for calibrating the data against inner- and intra-device variance was developed. The generalized region of interest model was used to determine the mobile phone's predicted bilirubin values. The results reported were a R^2 value of 0.15 and a limit of agreement of +10 mg/dL to -11 mg/dL. The results indicate a potential capability for the use of a mobile phone-based TcB device in LMIC, and inspire a further need for understanding models constructed from 2d spatially resolved images.

The third aim of this dissertation was to develop an understanding of the impact that spatial and spectral regions of interest from 2d spatially resolved diffuse reflectance has on multiple linear regression models. Optical tissue phantoms were designed to mimic the optical properties in the epithelial and dermal skin layers, which are important for taking bilirubin measurements. Three dimensions of variability were used to demonstrate the variability that melanin, bilirubin and hemoglobin has on model construction of 2d spatially resolved images. Linear regression models were constructed with varying spectral and spatial regions of interest. The results of this study suggest that 2d spatially resolved diffuse reflectance models benefit the most from unique spatial and spectral regions of interest.

The work completed in this dissertation has demonstrated the feasibility of a mobile phone-based TcB device that utilizes 2d spatially resolved imaging, and has laid a

basic foundation for performing mobile phone-based TcB studies in LMICs. However, additional device modifications and clinical work are necessary.

Mobile Phone-Based TcB

Aims 1 and 2 of this dissertation provided proof of concept of the feasibility of a mobile phone-based TcB approach. Broadly, this work has demonstrated the ability of mobile phone-based TcB devices that can perform transcutaneous measurements in clinical settings in high-income countries and low- and middle-income countries. The advantage of this approach is in its adaptability to be applied to widely accessible mobile phones at a low cost.

Spatially resolved diffuse reflectance measurements from neonatal skin falls off exponentially as a function of distance from the point of tissue illumination. The mobile phone-based TcB device required the selection of an integration time that provides signal information in the red, green and blue channels of the images, however prioritizing simple measurement protocol in Aim 1 and Aim 2 resulted in the choice to select a compromise value for the integration times which balanced undesirable oversaturation of the red and green channels against proper exposure of the blue channel, where the primary absorption peak of bilirubin resides. However, this limited the number of unique spatial and spectral channels that could be used in the multiple regression model for region of interest based 2d spatially resolved diffuse reflectance. While we were still able to construct models that predicted bilirubin values, it is clear that a wider range of properly exposed reflectance data would benefit regression model construction.

Alternative approaches such as high dynamic range images are a solution for acquiring images with evenly exposed color channels. This strategy would address the range of spatial reflectance data available for model construction. Additional factors that contribute to measurement variability include pressure sensitivity of measurements observed in benchtop scenarios, and standardization of data collection protocols to reduce user variability may also be beneficial in future studies.

In Aim 2, results from a large pilot study revealed a challenge for data to be aggregated together from 3 separate devices. Despite observations of high variability in clinical measurements, residual differences between individual device measurements persisted after images were calibrated. This may be due to a function of the calibration target used and how the device is used differently from person to person. The calibration target is a flat and hard white reflectance target; while the patient data varies from the target in optical chromophores and hardness. The patient measurements are collected on a semi-hard surface which subject the device measurements to additional variance based on the user. Approaches for addressing this issue include the creation of a mechanical nose on the device that clicks into position to standardize measurements or the modification of the mobile app with an alignment feature for point spread functions.

In Aim 3, results from a phantom study revealed that 2d spatially resolved diffuse reflectance models benefit the most from unique spatial and spectral regions of interest. While this study provides insightful information on how spatial and spectral resolved regions of interest impact multi-linear regression model construction from low and high coffee optical phantoms, further investigation is necessary for increased dimensions of

phantom optical chromophore variability. The variability considered for the optical chromophores used in the phantoms in this study are 3 concentrations of yellow dye, 3 concentrations of red dye and 2 concentrations of coffee. Clinical application of the mobile phone-based TcB device will need to consider optical chromophores that have higher dimension of complexity to fully assess model construction for bilirubin.

Future Direction

The primary motivation for the transformation of the mobile phone into a mobile phone-based TcB device was to create a widely accessible device that is capable of improving the management of NNJ in LMICs. This included screening, telehealth communication and disease tracking. The mobile phone-based TcB device has the capability to perform all of these tasks as feasibly shown in Aim 1 and 2. While the linear regression results reported in these aims were weak, they are not unexpected, as similar studies performed on African neonates demonstrated similar results. A unique aspect that the mobile phone-based TcB offers is that the ROI-based model can be modified to include more ROIs to help improve the regression model. However, this is unattainable with the current sample size. An increase of ROIs would lead to overparameterization of the model with the current sample size and ultimately be ungeneralizable. Further studies with increased sample size are required for further investigation of the impact of additional ROIs with this approach.

In order to further demonstrate the ability of this device, a small pilot study should be used to demonstrate the ability of this device to assist in the management of

screening and disease management in LMICs. The hypothesis is that the mobile phone TcB device can decrease symptoms to treatment times for neonates. This could be accomplished by partnering with local healthcare workers and clinics for the use of this device with neonates born outside the clinics. The mobile phone TcB device would be used in local villages where local screening of bilirubin levels would be conducted followed by directing patients to local clinics where they can be diagnosed and treated. This would demonstrate the device's ability to be used in wider settings and its ability to integrate into clinical settings.

The limitations demonstrated from Aim 1 of the current mobile phone-based TcB warrant the development of a second generation device, which is already underway. The second generation mobile phone device we selected is the OnePlus3000A, which was chosen due its common use in Kano, Nigeria. The added benefit of this device is that it carries more processing space to acquire more images. Modifications have been made to the mobile phone app to include additional measurements with varying exposure times. This was done to address limitations associated with the oversaturation and undersaturation of images collected with the first generation device. This improvement could be used to create high dynamic range images or the selection of images at the specific integration times that increase the performance of the regression model construction.

Beyond these basic study explorations of improvements made to this TcB approach, a reimagining of the physical approach may also be warranted. Each year mobile phones are constantly being updated and upgraded with many different optical

configurations. This decreases the adoptability of the mobile phone-based TcB device for usage between different models of mobile phones. While mobile phone applications offer a variety of advantages for different healthcare management systems, the unique changes to the camera and flash capabilities decrease the mobile phone adapters generalizability across multiple phones. Recently, it has become fairly simple to acquire LEDs and camera modules that can work in conjunction with arduinos. What may be more advantageous is to build a TcB device that utilizes both a camera module and LEDs and works in conjunction to the mobile phone with an app. This approach would limit the subjectivity to the changes made to mobile phones' camera and flash.

While not the first of its kind, the mobile phone-based TcB device represents an approach that has demonstrated feasibility for improvement of the management of neonatal jaundice in LMICs. However, it is the first demonstration for utilization of 2d spatially resolved diffuse reflectance to predict bilirubin measurements. The region of interest based generalized linear regression model signifies a unique approach to 2d diffuse reflectance based imaging. The spatially resolved diffuse reflectance with a mobile phone camera manuscript will signify the first to demonstrate analysis of the bilirubin concentration with a phantom study. Despite the limited range of chromophores used in this phantom study, general trends in spatial and spectral regions of interest for model construction were observed and provided valuable insight to future design considerations. While the primary product of this dissertation was for approaches associated with improving the management of neonatal jaundice in LMICs, the

approaches developed can be expanded to additional management of many transcutaneous-based diseases.

7. OUTPUTS AND DELIVERABLES

The work presented in this dissertation has led to several published papers, papers in preparation for publication, numerous conference proceedings and oral presentations. The outputs are listed in the following lists. Papers labeled with submission have been submitted for peer-review to scientific publications, documents labeled with “in preparation for submission” have been written and are presently in a state of internal review between myself and Dr. Chetan Patil.

Papers

B. Harrison, A. Dumont, M. Arefin, Y. Sun, J. So, S. Chandragiri, Z. McCormack, A. Nwaba, H. Weitkamp, A. Paed, Z. Farouk and C.A. Patil, “Development of a Mobile Phone Camera Based Transcutaneous Bilirubinometer for Low-Resource Settings” accepted by Biomedical Optics Express.

B. Harrison, A. Dumont, M. Shahriar, J. So, S. Chandragiri, Z. McCormack, A. Nwaba, H. Weitkamp, Z. Farouk, L. Nuraddeen, J. Perlman, R. Moshiro, J. Kim and C.A. Patil, “Feasibility Study of Mobile Phone-Based TCB Approach to Improving the Management of Neonatal Jaundice” in preparation to Scientific Reports.

B. Harrison, M. Arefin, H. Weitkamp, C. A. Patil, “2D Spatially Resolved Diffuse Reflectance Imaging with a Mobile Phone Camera”, for submission to Biomedical Optics Express.

Conference Abstracts/Proceedings

B. Harrison, A. Dumont, M. Arefin, and C.A. Patil, “Reducing Racial Bias in Transcutaneous Measurements with Mobile Phone Camera Based Spatially Resolved Diffuse Reflectance”, Optical Interactions with Tissue and Cells XXXIII and Advanced Photonics in Urology, 2022 SPIE Photonics West, San Francisco California January 22-23 (oral).

A.P Dumont, Y. Sun, B. Harrison, J. So, and C.A. Patil, "Validation of an Accelerated Raman Monte-Carlo Model for Determining Spatial and Spectral Thresholds for Calcification Detection in Tissues", BMES Annual Conference, October 16-19, 2019, Philadelphia, PA (poster).

B. Harrison, A.P. Dumont, Z. McCormick, A. Nwaba, S. Grossarth, H. Weitkamp, and C.A. Patil, "Development and Validation of a Mobile Phone Based Transcutaneous Bilirubinometer", BMES Annual Conference, October 16-19, 2019, Philadelphia, PA.

B. Harrison, A.P. Dumont, J. So, S. Chandragiri, A. Nwaba, S. Grossarth, Z. McCormick, H. Weitkamp, N. Lawal, A. Muhammed, Z.L. Farouk and C.A. Patil, "Development of a Mobile Phone Based Transcutaneous Bilirubinometer," Northeastern Biomedical Engineering Conference (NEBEC), March 20, 2019, New Brunswick, NJ (oral).

B. Harrison, A. Dumont, Z. McCormack, H. Weitkamp, and C.A. Patil, "Mobile Phone Based Transcutaneous Bilirubinometry Preclinical Study" Biomedical Engineering Society (BMES) Annual Conference, October 18, 2018, Atlanta, GA (poster).

Y. Sun, M. Haifler, B. Harrison, A.P. Dumont, and C.A. Patil, "Two-stage Local Outlier Factor for Multivariate Identification of Outliers in Optical Spectroscopy and Imaging", Biomedical Engineering Society (BMES) Annual Conference, October 18, 2018, Atlanta, GA (poster).

N. Mucciolo, K. Sareeram, B. Harrison, A. Dumont and C.A. Patil, "Development of New Reference Standards in Mobile Phone-Based Bilirubinometry", BMES annual conference, Atlanta GA, October 18, 2018. (poster).

B. Harrison, A. Dumont, Z. McCormack, A. Nwaba, H. Weitkamp, and C.A. Patil, "Development of the 2nd generation Mobile phone based transcutaneous bilirubinometer", Northeastern Biomedical Engineering Conference (NEBEC) March 30, 2018, Philadelphia, PA (oral).

B. Harrison, A. Dumont, Z. McCormack, H. Weitkamp, and C.A. Patil, "Mobile Phone Based Transcutaneous Bilirubinometry", Biophotonics in Low Resource Settings III, 2018 SPIE Photonics West, San Francisco California (oral).

J. So, S. Chanragiri, B. Harrison, A. Dumont, and C.A. Patil, "Optical Phantoms for Mobile Based Diagnosis" accept for poster presentation at BMES annual conference, Phoenix AZ, October 12-15, 2017.

A. Dumont, B. Harrison, Z.T. McCormick, N. Ganesh-Kumar, C.A. Patil, "Development of mobile phone based transcutaneous bilirubinometry" presented at Optics and Biophotonics in Low-Resource Settings III, SPIE Photonics West, San Francisco California, Jan 29, 2017 (oral).

BIBLIOGRAPHY

- [1] J. T. Walsh, “Basic interactions of light with tissue,” *Optical-Thermal Response of Laser-Irradiated Tissue*, pp. 13–26, 2011, doi: 10.1007/978-90-481-8831-4_2.
- [2] Aaron Lee, “The EM Spectrum – Basic Lighting for Electricians: Level 1.” <https://pressbooks.bccampus.ca/lightingforelectricians/chapter/the-em-spectrum/> (accessed Mar. 27, 2022).
- [3] P. D. Mannheimer, “The light-tissue interaction of pulse oximetry,” *Anesthesia and Analgesia*, vol. 105, no. SUPPL. 6, 2007, doi: 10.1213/01.ane.0000269522.84942.54.
- [4] P. N. Prasad, “Introduction to Biophotonics,” *Introduction to Biophotonics*, Apr. 2003, doi: 10.1002/0471465380.
- [5] M. A. Golshan, M. G. Tarei, M. A. Ansari, and A. Amjadi, “The Propagation of Laser Light in Skin by Monte Carlo- Diffusion Method : A Fast and Accurate Method to Simulate Photon Migration in Biological Tissues,” vol. 2, no. 3, pp. 109–114, 2011.
- [6] A. Méndez, “Optics in medicine,” *Optics in Our Time*, pp. 299–333, Jan. 2016, doi: 10.1007/978-3-319-31903-2_13/FIGURES/38.
- [7] A. J. Welch and M. J. C. Van Gemert, “Introduction to medical applications,” *Optical-Thermal Response of Laser-Irradiated Tissue*, pp. 653–659, 2011, doi: 10.1007/978-90-481-8831-4_16.

- [8] N. G. Khlebtsov, I. L. Maksimova, I. Meglinski, L. V. Wang, and V. V. Tuchin, “Introduction to Light Scattering by Biological Objects,” *Handbook of Optical Biomedical Diagnostics, Second Edition, Volume 1: Light-Tissue Interaction*, Jan. 2017, doi: 10.1117/3.2219603.CH1.
- [9] G. A. Langmann, K. T. Vujevich, D. Medich, M. E. Miller, and S. L. Greenspan, “Women with Breast Cancer,” vol. 15, no. 3, pp. 290–294, 2016, doi: 10.1016/j.jocd.2012.01.008.Heel.
- [10] B. J. Tromberg, L. O. Svaasand, T. Spott, and T. H. Pham, “Quantifying the properties of two-layer turbid media with frequency-domain diffuse reflectance,” *Applied Optics, Vol. 39, Issue 25, pp. 4733-4745*, vol. 39, no. 25, pp. 4733–4745, Sep. 2000, doi: 10.1364/AO.39.004733.
- [11] G. Xu *et al.*, “Photoacoustic spectrum analysis for microstructure characterization in biological tissue: Analytical model,” *Ultrasound in Medicine and Biology*, vol. 41, no. 5, pp. 1473–1480, 2015, doi: 10.1016/j.ultrasmedbio.2015.01.010.
- [12] S. B. Munkholm, T. Krøgholt, F. Ebbesen, P. B. Szecsi, and S. R. Kristensen, “The smartphone camera as a potential method for transcutaneous bilirubin measurement,” *PLoS ONE*, vol. 13, no. 6, Jun. 2018, doi: 10.1371/journal.pone.0197938.
- [13] D. Reflectance and P. Samples, “Diffuse Reflectance – Theory and Applications,” 2011.

- [14] G. Zonios and A. Dimou, "Modeling diffuse reflectance from semi-infinite turbid media: application to the study of skin optical properties," *Optics Express*, vol. 14, no. 19, p. 8661, 2006, doi: 10.1364/oe.14.008661.
- [15] D. Reflectance and P. Samples, "Diffuse Reflectance – Theory and Applications," 2011.
- [16] I. Nishidate, C. Mizushima, K. Yoshida, S. Kawauchi, S. Sato, and M. Sato, "In vivo estimation of light scattering and absorption properties of rat brain using a single-reflectance fiber probe during cortical spreading depression," *J Biomed Opt*, vol. 20, no. 2, p. 027003, Feb. 2015, doi: 10.1117/1.JBO.20.2.027003.
- [17] O. Senlik and N. M. Jokerst, "Concentric multipixel silicon photodiode array probes for spatially resolved diffuse reflectance spectroscopy," *IEEE Journal of Selected Topics in Quantum Electronics*, vol. 22, no. 3, pp. 7–12, May 2016, doi: 10.1109/JSTQE.2015.2505733.
- [18] D. J. Cappon, T. J. Farrell, Q. Fang, and J. E. Hayward, "Fiber-optic probe design and optical property recovery algorithm for optical biopsy of brain tissue," *Journal of Biomedical Optics*, 2013, doi: 10.1117/1.JBO.18.10.107004.
- [19] Z. Shi and C. A. Anderson, "Pharmaceutical applications of separation of absorption and scattering in near-infrared spectroscopy (NIRS)," *Journal of Pharmaceutical Sciences*, vol. 99, no. 12, pp. 4766–4783, 2010, doi: 10.1002/jps.22228.
- [20] M. N. Kholodtsova *et al.*, "Spatially and spectrally resolved particle swarm optimization for precise optical property estimation using diffuse-reflectance

- spectroscopy,” *Phys. Med. Biol.*, vol. 45, no. 5, p. 1127, 2000, doi: 10.1364/OE.24.012682.
- [21] D. J. Evers *et al.*, “Optical sensing for tumor detection in the liver,” *Eur J Surg Oncol*, vol. 39, no. 1, pp. 68–75, Jan. 2013, doi: 10.1016/J.EJSO.2012.08.005.
- [22] S. Fan, R. Cai, W. Xing, C. Liu, G. Chen, and J. Wang, “An analysis on the theory of pulse oximetry by Monte Carlo simulation,” <https://doi.org/10.1117/12.806731>, vol. 7128, pp. 371–376, Oct. 2008, doi: 10.1117/12.806731.
- [23] J. C. Finlay and T. H. Foster, “Hemoglobin oxygen saturations in phantoms and in vivo from measurements of steady-state diffuse reflectance at a single, short source-detector separation,” *Medical Physics*, vol. 31, no. 7, pp. 1949–1959, 2004, doi: 10.1118/1.1760188.
- [24] M. Sharma, R. Hennessy, M. K. Markey, and J. W. Tunnell, “Verification of a two-layer inverse Monte Carlo absorption model using multiple source-detector separation diffuse reflectance spectroscopy,” *Biomedical Optics Express*, vol. 5, no. 1, p. 40, 2014, doi: 10.1364/boe.5.000040.
- [25] R. M. P. Doornbos, R. Lang, M. C. Aalders, F. W. Cross, and H. J. C. M. Sterenborg, “The determination of in vivo human tissue optical properties and absolute chromophore concentrations using spatially resolved steady-state diffuse reflectance spectroscopy,” *Physics in Medicine and Biology*, vol. 44, no. 4, pp. 967–981, 1999, doi: 10.1088/0031-9155/44/4/012.

- [26] M. W. Sjoding *et al.*, “Racial bias in accuracy of pulse oximetry and its impact on assessments of hypopnea and T90 in clinical studies,” *Journal of Clinical Sleep Medicine*, vol. 17, no. 5, p. 1145, May 2021, doi: 10.5664/JCSM.9178.
- [27] M. W. Sjoding, R. P. Dickson, T. J. Iwashyna, S. E. Gay, and T. S. Valley, “Racial Bias in Pulse Oximetry Measurement,” *New England Journal of Medicine*, vol. 383, no. 25, pp. 2477–2478, Dec. 2020, doi: 10.1056/NEJMC2029240/SUPPL_FILE/NEJMC2029240_DISCLOSURES.PDF.
- [28] X. He, D. Hu, X. Fu, and X. Rao, “Spatial frequency domain imaging for determining absorption and scattering properties of bruised pears based on profile corrected diffused reflectance,” *Postharvest Biology and Technology*, vol. 179, p. 111570, Sep. 2021, doi: 10.1016/J.POSTHARVBIO.2021.111570.
- [29] S. Gioux, A. Mazhar, and D. J. Cuccia, “Spatial frequency domain imaging in 2019: principles, applications, and perspectives,” <https://doi.org/10.1117/1.JBO.24.7.071613>, vol. 24, no. 7, p. 071613, Jun. 2019, doi: 10.1117/1.JBO.24.7.071613.
- [30] B. J. Tromberg *et al.*, “Non-Invasive In Vivo Characterization of Breast Tumors Using Photon Migration Spectroscopy,” *Neoplasia*, vol. 2, no. 1–2, p. 26, 2000, doi: 10.1038/SJ.NEO.7900082.
- [31] K. Huang, S. Li, X. Kang, and L. Fang, “Spectral–Spatial Hyperspectral Image Classification Based on KNN,” *Sensing and Imaging*, vol. 17, no. 1, pp. 1–13, Dec. 2016, doi: 10.1007/S11220-015-0126-Z/TABLES/2.

- [32] R. P. Singh-Moon, D. M. Roblyer, I. J. Bigio, and S. Joshi, “Spatial mapping of drug delivery to brain tissue using hyperspectral spatial frequency-domain imaging,” <https://doi.org/10.1117/1.JBO.19.9.096003>, vol. 19, no. 9, p. 096003, Sep. 2014, doi: 10.1117/1.JBO.19.9.096003.
- [33] L. Hoogedoorn, M. Peppelman, P. C. M. van de Kerkhof, P. E. J. van Erp, and M. J. P. Gerritsen, “The value of *in vivo* reflectance confocal microscopy in the diagnosis and monitoring of inflammatory and infectious skin diseases: a systematic review,” *British Journal of Dermatology*, vol. 172, no. 5, pp. 1222–1248, 2015, doi: 10.1111/bjd.13499.
- [34] S. L. Jacques, “The Role of Skin Optics in Diagnostic and Therapeutic Uses of Lasers,” *Lasers in Dermatology*, pp. 1–21, 1991, doi: 10.1007/978-3-642-75201-8_1.
- [35] A. J. Moy and J. W. Tunnell, “Diffuse Reflectance Spectroscopy and Imaging,” *Imaging in Dermatology*, pp. 203–215, Aug. 2016, doi: 10.1016/B978-0-12-802838-4.00017-0.
- [36] E. A. Edwards and S. Q. Duntley, “The pigments and color of living human skin,” *Am. J. Anat.*, vol. 65, no. 1, pp. 1–33, Jul. 1939, doi: 10.1002/aja.1000650102.
- [37] E. Proksch, J. M. Brandner, and J. M. Jensen, “The skin: An indispensable barrier,” *Experimental Dermatology*, vol. 17, no. 12, pp. 1063–1072, 2008, doi: 10.1111/J.1600-0625.2008.00786.X.
- [38] Dr. Bobby Buka, “Skin Anatomy 101 - The Dermatology Specialists.” <https://www.thedermspecs.com/blog/skin-anatomy-101/> (accessed Mar. 28, 2022).

- [39] M. Visscher and S. S. Program, “Neonatal Skin Physiology,” no. May, 2011.
- [40] P. M. Varughese, L. Krishnan, and Ravichandran, “Does color really matter? Reliability of transcutaneous bilirubinometry in different skin-colored babies,” *Indian Journal of Paediatric Dermatology*, vol. 19, no. 4, p. 315, 2018, doi: 10.4103/IJPD.IJPD_3_18.
- [41] S. N. El-Beshbishi, K. E. Shattuck, A. A. Mohammad, and J. R. Petersen, “Hyperbilirubinemia and Transcutaneous Bilirubinometry,” 2009, doi: 10.1373/clinchem.2008.121889.
- [42] B. J. Lauer and N. D. Spector, “Hyperbilirubinemia in the Newborn,” *Pediatrics in Review*, vol. 32, no. 8, pp. 341 LP – 349, Aug. 2011, [Online]. Available: <http://pedsinreview.aappublications.org/content/32/8/341.abstract>
- [43] T. M. Slusher *et al.*, “Transcutaneous bilirubin measurements and serum total bilirubin levels in indigenous African infants,” *Pediatrics*, vol. 113, no. 6 I, pp. 1636–1641, Jun. 2004, doi: 10.1542/peds.113.6.1636.
- [44] J. P. Haydek *et al.*, “Extreme hyperbilirubinemia: An indicator of morbidity and mortality in sickle cell disease,” *World Journal of Hepatology*, vol. 11, no. 3, p. 287, Mar. 2019, doi: 10.4254/WJH.V11.I3.287.
- [45] Nasional Insitute for health and Exellence, “Neonatal jaundice.,” *MidCity Place*, vol. 5, no. May, pp. 457–475, 2010, doi: 10.1093/tropej/fms051.
- [46] Z. L. Farouk, A. Muhammed, S. Gambo, M. Mukhtar-Yola, S. Umar Abdullahi, and T. M. Slusher, “Follow-up of Children with Kernicterus in Kano, Nigeria,” *J Trop Pediatr*, vol. 64, no. 3, pp. 176–182, 2018, doi: 10.1093/TROPEJ/FMX041.

- [47] W. D. Engle, G. L. Jackson, D. Sendelbach, D. Manning, and W. H. Frawley, “Assessment of a transcutaneous device in the evaluation of neonatal hyperbilirubinemia in a primarily Hispanic population,” *Pediatrics*, vol. 110, no. 1 I, pp. 61–67, 2002, doi: 10.1542/peds.110.1.61.
- [48] S. M. Johnson *et al.*, “Validation of transcutaneous bilirubinometry during phototherapy for detection and monitoring of neonatal jaundice in a low-income setting,” *Paediatrics and International Child Health*, vol. 00, no. 00, pp. 1–5, 2019, doi: 10.1080/20469047.2019.1598126.
- [49] M. Radfar, M. Hashemieh, F. Shirvani, and R. Madani, “Transcutaneous bilirubinometry in preterm and term newborn infants before and during phototherapy,” *Archives of Iranian Medicine*, vol. 19, no. 5, pp. 323–328, 2016.
- [50] A. Bastawrous and M. J. Armstrong, “Mobile health use in low-and high-income countries: An overview of the peer-reviewed literature,” *J R Soc Med*, vol. 106, no. 4, pp. 130–142, 2013, doi: 10.1177/0141076812472620.
- [51] L. de Greef *et al.*, “Bilicam: using mobile phones to monitor newborn jaundice,” *Proceedings of the 2014 ACM International Joint Conference on Pervasive and Ubiquitous Computing*, pp. 331–342, 2014, doi: 10.1145/2632048.2632076.
- [52] D. Fricke, E. Denker, A. Heratizadeh, T. Werfel, M. Wollweber, and B. Roth, “Non-Contact Dermatoscope with Ultra-Bright Light Source and Liquid Lens-Based Autofocus Function,” *Applied Sciences 2019, Vol. 9, Page 2177*, vol. 9, no. 11, p. 2177, May 2019, doi: 10.3390/APP9112177.

- [53] G. Inamori *et al.*, “Neonatal wearable device for colorimetry-based real-time detection of jaundice with simultaneous sensing of vitals,” *Science Advances*, vol. 7, no. 10, Mar. 2021, doi: 10.1126/SCIADV.ABE3793.
- [54] V. I. Bhutani and L. H. Johnson, “Newborn Jaundice and Kernicterus-Health and Societal Perspectives,” Philadelphia, 2003.
- [55] C. Greco *et al.*, “Neonatal Jaundice in Low- and Middle-Income Countries: Lessons and Future Directions from the 2015 Don Ostrow Trieste Yellow Retreat,” *Neonatology*, vol. 110, no. 3, pp. 172–180, 2016, doi: 10.1159/000445708.
- [56] V. K. Bhutani *et al.*, “Neonatal hyperbilirubinemia and rhesus disease of the newborn: Incidence and impairment estimates for 2010 at regional and global levels,” *Pediatric Research*, vol. 74, no. SUPPL. 1, pp. 86–100, 2013, doi: 10.1038/pr.2013.208.
- [57] B. O. Olusanya, A. A. Emokpae, T. G. Zamora, and T. M. Slusher, “Addressing the burden of neonatal hyperbilirubinaemia in countries with significant glucose-6-phosphate dehydrogenase deficiency,” *Acta Paediatrica, International Journal of Paediatrics*, vol. 103, no. 11. Blackwell Publishing Ltd, pp. 1102–1109, Nov. 01, 2014. doi: 10.1111/apa.12735.
- [58] B. O. Olusanya, T. A. Ogunlesi, and T. M. Slusher, “Why is kernicterus still a major cause of death and disability in low-income and middle-income countries?,” *Archives of Disease in Childhood: Education and Practice Edition*, vol. 99, no. 12, pp. 1117–1121, Dec. 2014, doi: 10.1136/archdischild-2013-305506.

- [59] T. M. Slusher *et al.*, “Burden of severe neonatal jaundice: a systematic review and meta-analysis,” *BMJ Paediatrics Open*, vol. 1, no. 1, 2017, doi: 10.1136/BMJPO-2017-000105.
- [60] Z. L. Farouk, T. M. Slusher, A. A. Danzomo, and I. L. Slusher, “Knowledge, Observation and Practices Related to Neonatal Jaundice in a Rural Community in Kano, Nigeria,” *Journal of Tropical Pediatrics*, vol. 67, no. 1, Jan. 2021, doi: 10.1093/TROPEJ/FMAA134.
- [61] Z. L. Farouk, F. Usman, B. M. Musa, V. C. Ezeaka, and A. Okolo, “Societal awareness on neonatal hyperbilirubinemia: A systematic review and meta-analysis,” *Seminars in Perinatology*, vol. 45, no. 1, p. 151361, 2021, doi: 10.1016/J.SEMPERI.2020.151361.
- [62] P. A. Keahey *et al.*, “Point-of-care device to diagnose and monitor neonatal jaundice in low-resource settings,” *Proc Natl Acad Sci U S A*, vol. 114, no. 51, pp. E10965–E10971, 2017, doi: 10.1073/pnas.1714020114.
- [63] C. D. C. Zabetta *et al.*, “Bilistick: A low-cost point-of-care system to measure total plasma bilirubin,” *Neonatology*, vol. 103, no. 3, pp. 177–181, 2013, doi: 10.1159/000345425.
- [64] B. Rolinski, H. Kuster, B. Ugele, R. Gruber, and K. Horn, “Total Bilirubin Measurement by Photometry on a Blood Gas Analyzer: Potential for Use in Neonatal Testing at the Point of Care,” *Clinical Chemistry*, vol. 47, no. 10, pp. 1845–1847, Oct. 2001, doi: 10.1093/clinchem/47.10.1845.

- [65] R. S. Tabatabaee, H. Golmohammadi, and S. H. Ahmadi, "Easy Diagnosis of Jaundice: A Smartphone-Based Nanosensor Bioplatfrom Using Photoluminescent Bacterial Nanopaper for Point-of-Care Diagnosis of Hyperbilirubinemia," *ACS Sensors*, vol. 4, no. 4, pp. 1063–1071, 2019, doi: 10.1021/acssensors.9b00275.
- [66] W. D. Engle, G. L. Jackson, and N. G. Engle, "Transcutaneous bilirubinometry," *Seminars in Perinatology*, vol. 38, no. 7. W.B. Saunders, pp. 438–451, 2014. doi: 10.1053/j.semperi.2014.08.007.
- [67] M. Jeffrey Maisels *et al.*, "Evaluation of a New Transcutaneous Bilirubinometer," Michigan, 2004. [Online]. Available: www.aappublications.org/news
- [68] V. K. Bhutani and L. Johnson, "A proposal to prevent severe neonatal hyperbilirubinemia and kernicterus," *Journal of Perinatology*, vol. 29, no. 1. Nature Publishing Group, pp. S61–S67, 2009. doi: 10.1038/jp.2008.213.
- [69] V. K. Bhutani, R. J. Vilms, and L. Hamerman-Johnson, "Universal bilirubin screening for severe neonatal hyperbilirubinemia," *Journal of Perinatology*, vol. 30, no. SUPPL. 1, 2010, doi: 10.1038/jp.2010.98.
- [70] S. on Hyperbilirubinemia, "Management of Hyperbilirubinemia in the Newborn Infant 35 or More Weeks of Gestation," *Pediatrics*, vol. 114, no. 1, pp. 297–316, Jul. 2004, doi: 10.1542/PEDS.114.1.297.
- [71] B. L. Burke, J. M. Robbins, T. mac Bird, C. A. Hobbs, C. Nesmith, and J. M. Tilford, "Trends in hospitalizations for neonatal jaundice and kernicterus in the United States, 1988-2005," *Pediatrics*, vol. 123, no. 2, pp. 524–532, Feb. 2009, doi: 10.1542/peds.2007-2915.

- [72] J. A. Taylor *et al.*, “Use of a smartphone app to assess neonatal jaundice,” *Pediatrics*, vol. 140, no. 3, 2017, doi: 10.1542/peds.2017-0312.
- [73] S. Tachakra, X. H. Wang, R. S. H. Istepanian, and Y. H. Song, “Mobile e-Health: The Unwired Evolution of Telemedicine,” *Telemedicine Journal and e-Health*, vol. 9, no. 3, pp. 247–257, 2003, doi: 10.1089/153056203322502632.
- [74] D. N. Breslauer, R. N. Maamari, N. A. Switz, W. A. Lam, and D. A. Fletcher, “Mobile phone based clinical microscopy for global health applications,” *PLoS ONE*, vol. 4, no. 7, pp. 1–7, 2009, doi: 10.1371/journal.pone.0006320.
- [75] R. Braun, V. JL, L. Thomas, and et al, “Telemedical wound care using a new generation of mobile telephones: A feasibility study,” *Archives of Dermatology*, vol. 141, no. 2, pp. 254–258, Feb. 2005, [Online]. Available: <http://dx.doi.org/10.1001/archderm.141.2.254>
- [76] S. L. Jacques and D. G. Oelberg, “United States Patent 19 Jacques Steven. 54 METHOD AND APPARATUS FOR OPTICAL MEASUREMENT OF BILIRUBIN IN TISSUE,” Austin , Jan. 1992.
- [77] J. A. D. Atencio, E. E. Rodríguez, A. C. Rodríguez, and J. F. Rivas-Silva, “Monte Carlo simulation of visible light diffuse reflection in neonatal skin,” in *AIP Conference Proceedings*, 2008, vol. 992, no. 1, pp. 1156–1159. doi: 10.1063/1.2926810.
- [78] A. P. Dumont, B. Harrison, Z. T. McCormick, N. Ganesh Kumar, and C. A. Patil, “Development of mobile phone based transcutaneous bilirubinometry,” *Biomedical Optics*, vol. 10055, p. 100550T, Mar. 2017, doi: 10.1117/12.2257428.

- [79] A. P. Dumont, Q. Fang, and C. A. Patil, "A computationally efficient Monte-Carlo model for biomedical Raman spectroscopy," *Journal of Biophotonics*, vol. 14, no. 7, p. e202000377, Jul. 2021, doi: 10.1002/JBIO.202000377.
- [80] D. A. Boas and Q. Fang, "Monte Carlo Simulation of Photon Migration in 3D Turbid Media Accelerated by Graphics Processing Units," *Optics Express*, Vol. 17, Issue 22, pp. 20178-20190, vol. 17, no. 22, pp. 20178–20190, 2009, doi: 10.1364/OE.17.020178.
- [81] Semrock, "Cleaning Optical Filters - Semrock."
<https://www.semrock.com/cleaning-optical-filters.aspx> (accessed Feb. 05, 2022).
- [82] E. Pawar, "A Review Article on Acrylic PMMA," *IOSR-JMCE*, vol. 13, no. 2, pp. 1–04, 2016, doi: 10.9790/1684-1302010104.
- [83] H. A. Vrooman *et al.*, "Multi-spectral brain tissue segmentation using automatically trained k-Nearest-Neighbor classification," *Neuroimage*, vol. 37, no. 1, pp. 71–81, Aug. 2007, doi: 10.1016/J.NEUROIMAGE.2007.05.018.
- [84] "Find minimum of function using pattern search - MATLAB patternsearch," 2021.
<https://www.mathworks.com/help/gads/patternsearch.html> (accessed Oct. 28, 2021).
- [85] P. Comtois, "The gamma distribution as the true aerobiological probability density function (PDF)," *Aerobiologia 2000 16:2*, vol. 16, no. 2, pp. 171–176, 2000, doi: 10.1023/A:1007667531246.

- [86] L. H. Moulton and S. L. Zeger, “Bootstrapping generalized linear models,” *Computational Statistics & Data Analysis*, vol. 11, no. 1, pp. 53–63, Jan. 1991, doi: 10.1016/0167-9473(91)90052-4.
- [87] S. Aouada, D. Traskov, N. D’Heureuse, and A. M. Zoubir, “Application of the bootstrap to source detection in nonuniform noise,” *ICASSP, IEEE International Conference on Acoustics, Speech and Signal Processing - Proceedings*, vol. IV, pp. 997–1000, 2005, doi: 10.1109/ICASSP.2005.1416179.
- [88] T. M. Slusher and Y. E. Vaucher, “Management of neonatal jaundice in low- and middle-income countries,” *Paediatrics and International Child Health*, vol. 40, no. 1. Taylor and Francis Ltd., pp. 7–10, 2020. doi: 10.1080/20469047.2019.1707397.
- [89] J. C. Aker and I. M. Mbiti, “Mobile Phones and Economic Development in Africa,” *Journal of Economic Perspectives*, vol. 24, no. 3, pp. 207–232, 2010, doi: 10.1257/JEP.24.3.207.
- [90] E. (Hooman) Banaei, “EVERIX, Inc.: Thermal Draw Process,” <https://doi.org/10.1117/12.2595964>, vol. 11716, p. 117160M, Mar. 2021, doi: 10.1117/12.2595964.
- [91] F. Raimondi *et al.*, “Measuring transcutaneous bilirubin: a comparative analysis of three devices on a multiracial population,” *BMC Pediatrics*, vol. 12, Jun. 2012, doi: 10.1186/1471-2431-12-70.
- [92] D. M. Campbell *et al.*, “Transcutaneous bilirubin measurement at the time of hospital discharge in a multiethnic newborn population,” Toronto, 2011.

- [93] C. M. aria Conceição, M. F. ernanda P. da S. Dornaus, M. A. parecida Portella, A. D. A. Deutsch, and C. M. oura Rebello, “Influence of assessment site in measuring transcutaneous bilirubin,” *Einstein (São Paulo, Brazil)*, vol. 12, no. 1, pp. 11–15, 2014, doi: 10.1590/S1679-45082014AO2711.
- [94] V. K. Bhutani, G. R. Gourley, S. Adler, B. Kreamer, C. Dalin, and L. H. Johnson, “Noninvasive measurement of total serum bilirubin in a multiracial predischarge newborn population to assess the risk of severe hyperbilirubinemia.,” *Pediatrics*, vol. 106, no. 2, p. 2021, Aug. 2000, doi: 10.1542/peds.106.2.e17.
- [95] B. O. Olusanya, D. O. Imosemi, and A. A. Emokpae, “Differences between transcutaneous and serum bilirubin measurements in black African neonates,” *Pediatrics*, vol. 138, no. 3, 2016, doi: 10.1542/peds.2016-0907.
- [96] B. O. Olusanya, C. A. Mabogunje, D. O. Imosemi, and A. A. Emokpae, “Transcutaneous bilirubin nomograms in African neonates,” *PLoS ONE*, vol. 12, no. 2, 2017, doi: 10.1371/JOURNAL.PONE.0172058.
- [97] C. D. Coda Zabetta *et al.*, “Bilistick: A Low-Cost Point-of-Care System to Measure Total Plasma Bilirubin,” *Neonatology*, vol. 103, no. 3, pp. 177–181, Mar. 2013, doi: 10.1159/000345425.
- [98] O. Senlik, G. Greening, T. J. Muldoon, and N. M. Jokerst, “Spatially resolved diffuse reflectance spectroscopy of two-layer turbid media by densely packed multi-pixel photodiode reflectance probe,” <https://doi.org/10.1117/12.2213124>, vol. 9700, pp. 108–113, Mar. 2016, doi: 10.1117/12.2213124.

- [99] M. S. Patterson, B. C. Wilson, and D. R. Wyman, “The Propagation of Optical Radiation in Tissue. II: Optical Properties of Tissues and Resulting Fluence Distributions,” *Lasers in Medical Science*, vol. 6, pp. 379–390, 1991.
- [100] G. Kortüm, W. Braun, and G. Herzog, “Principles and Techniques of Diffuse-Reflectance Spectroscopy,” *Angewandte Chemie International Edition in English*, vol. 2, no. 7, pp. 333–341, Jul. 1963, doi: 10.1002/ANIE.196303331.
- [101] L. Wang, S. L. Jacques, and L. Zheng, “MCML—Monte Carlo modeling of light transport in multi-layered tissues,” *Computer Methods and Programs in Biomedicine*, vol. 47, no. 2, pp. 131–146, Jul. 1995, doi: 10.1016/0169-2607(95)01640-F.
- [102] H. Nilsson, M. Larsson, G. E. Nilsson, and T. Stroemberg, “Photon pathlength determination based on spatially resolved diffuse reflectance,” <https://doi.org/10.1117/1.1482378>, vol. 7, no. 3, pp. 478–485, Jul. 2002, doi: 10.1117/1.1482378.
- [103] A. Kienle, L. Lilge, M. S. Patterson, R. Hibst, R. Steiner, and B. C. Wilson, “Spatially resolved absolute diffuse reflectance measurements for noninvasive determination of the optical scattering and absorption coefficients of biological tissue,” *Appl Opt*, vol. 35, no. 13, p. 2304, May 1996, doi: 10.1364/AO.35.002304.
- [104] B. Harrison-Smith *et al.*, “Development of a mobile phone camera-based transcutaneous bilirubinometer for low-resource settings,” *Biomedical Optics Express*, vol. 13, no. 5, pp. 2797–2809, May 2022, doi: 10.1364/BOE.449625.

- [105] M. Amouroux, W. C. P. M. Blondel, F. Granel-Brocard, F. Marchal, and F. Guillemin, “A preliminary study on skin phantoms to test spatially resolved - Diffuse Reflectance Spectroscopy as a tool to help diagnose cutaneous melanoma: A non-invasive measurement of Breslow index,” *Bio-Medical Materials and Engineering*, vol. 18, no. 4–5, pp. 339–343, 2008, doi: 10.3233/BME-2008-0550.
- [106] S. K. Loyalka and C. A. Riggs, “Inverse Problem in Diffuse Reflectance Spectroscopy: Accuracy of the Kubelka-Munk Equations,” *Appl. Spectrosc.* 49, 1995. <https://opg.optica.org/as/viewmedia.cfm?uri=as-49-8-1107&seq=0> (accessed Mar. 29, 2022).
- [107] B. H. Hokr and J. N. Bixler, “Machine learning estimation of tissue optical properties,” *Scientific Reports* /, vol. 11, p. 6561, 123AD, doi: 10.1038/s41598-021-85994-w.
- [108] G.-J. Qi and J. Luo, “Small Data Challenges in Big Data Era: A Survey of Recent Progress on Unsupervised and Semi-Supervised Methods; Small Data Challenges in Big Data Era: A Survey of Recent Progress on Unsupervised and Semi-Supervised Methods,” *IEEE Transactions on Pattern Analysis and Machine Intelligence*, vol. 44, 2022, doi: 10.1109/TPAMI.2020.3031898.
- [109] D. Pietersma, R. Lacroix, D. Lefebvre, and K. M. Wade, “Performance analysis for machine-learning experiments using small data sets,” *Computers and Electronics in Agriculture*, vol. 38, no. 1, pp. 1–17, Jan. 2003, doi: 10.1016/S0168-1699(02)00104-7.

- [110] K. A. Brown, S. Brittman, D. Jariwala, and U. Celano, “Machine Learning in Nanoscience: Big Data at Small Scales,” *Nano Lett*, vol. 20, no. 2, 2020, doi: 10.1021/acs.nanolett.9b04090.
- [111] T. S. Cohen and M. Welling MWELLING, “Group Equivariant Convolutional Networks,” 2016.
- [112] L. E. Eberly, “Multiple Linear Regression,” *Methods Mol Biol*, vol. 404, pp. 165–187, 2007, doi: 10.1007/978-1-59745-530-5_9.
- [113] K. A. Marill, “Advanced Statistics: Linear Regression, Part II: Multiple Linear Regression,” *Academic Emergency Medicine*, vol. 11, no. 1, pp. 94–102, 2004, doi: 10.1197/j.aem.2003.09.006.
- [114] S. Weisberg, *Applied linear regression*. Wiley-Interscience, 2005.
- [115] H. Martens and E. Stark, “Extended multiplicative signal correction and spectral interference subtraction: New preprocessing methods for near infrared spectroscopy,” *Journal of Pharmaceutical and Biomedical Analysis*, vol. 9, no. 8, pp. 625–635, 1991, doi: 10.1016/0731-7085(91)80188-F.
- [116] Y. N. Mirabal, S. K. Chang, E. N. Atkinson, A. M. M.D., M. Follen, and R. R. Richards-Kortum, “Reflectance spectroscopy for in vivo detection of cervical precancer,” <https://doi.org/10.1117/1.1502675>, vol. 7, no. 4, pp. 587–594, Oct. 2002, doi: 10.1117/1.1502675.
- [117] A. Amelink, O. P. Kaspers, H. J. C. M. Sterenborg, J. E. van der Wal, J. L. N. Roodenburg, and M. J. H. Witjes, “Non-invasive measurement of the morphology

- and physiology of oral mucosa by use of optical spectroscopy,” *Oral Oncology*, vol. 44, pp. 65–71, 2007, doi: 10.1016/j.oraloncology.2006.12.011.
- [118] A. Sharwani *et al.*, “Assessment of oral premalignancy using elastic scattering spectroscopy,” *Oral Oncology*, vol. 42, pp. 343–349, 2006, doi: 10.1016/j.oraloncology.2005.08.008.
- [119] V. T. C. Chang, P. S. Cartwright, S. M. Bean, G. M. Palmer, R. C. Bentley, and N. Ramanujam, “Quantitative physiology of the precancerous cervix in vivo through optical spectroscopy,” *Neoplasia*, vol. 11, no. 4, pp. 325–332, 2009, doi: 10.1593/NEO.81386.
- [120] J. Rennie, S. Burman-Roy, and M. S. Murphy, “Neonatal jaundice: summary of NICE guidance,” *BMJ*, vol. 340, no. 7757, pp. 1190–1191, May 2010, doi: 10.1136/BMJ.C2409.
- [121] G. L. T. Chimhini, S. Chimhuya, and V. Chikwasha, “Evaluation of transcutaneous bilirubinometer (DRAEGER JM 103) use in Zimbabwean newborn babies,” *Maternal Health, Neonatology and Perinatology*, vol. 4, no. 1, pp. 1–7, Dec. 2018, doi: 10.1186/s40748-017-0070-0.
- [122] J. R. Cook, R. R. Bouchard, and S. Y. Emelianov, “Tissue-mimicking phantoms for photoacoustic and ultrasonic imaging,” *Biomedical Optics Express*, vol. 2, no. 11, p. 3193, 2011, doi: 10.1364/BOE.2.003193.
- [123] N. Bosschaart, R. Mentink, A. G. J. M. T. van Leeuwen, M. C. G. Aalders, and J. H. Kok, “Optical properties of neonatal skin measured in vivo as a function of age

and skin pigmentation,” <https://doi.org/10.1117/1.3622629>, vol. 16, no. 9, p. 097003, Sep. 2011, doi: 10.1117/1.3622629.

- [124] K. sun Lee, L. M. Gartner, and I. Zarafu, “Fluorescent dye method for determination of the bilirubin-binding capacity of serum albumin,” *The Journal of Pediatrics*, vol. 86, no. 2, pp. 280–285, 1975, doi: 10.1016/S0022-3476(75)80489-6.
- [125] R. B. Saager, C. Kondru, K. Au, K. Sry, F. Ayers, and A. J. Durkin, “Multilayer silicone phantoms for the evaluation of quantitative optical techniques in skin imaging,” <https://doi.org/10.1117/12.842249>, vol. 7567, pp. 40–47, Feb. 2010, doi: 10.1117/12.842249.
- [126] D. M. de Bruin *et al.*, “Optical phantoms of varying geometry based on thin building blocks with controlled optical properties,” *Journal of Biomedical Optics*, vol. 15, no. 2, p. 25001, 2010, doi: 10.1117/1.3369003.
- [127] V. K. Bhutani *et al.*, “Neonatal hyperbilirubinemia and rhesus disease of the newborn: Incidence and impairment estimates for 2010 at regional and global levels,” *Pediatric Research*, vol. 74, no. SUPPL. 1, pp. 86–100, 2013, doi: 10.1038/pr.2013.208.
- [128] S. L. Jacques and D. G. Oelberg, “Method and apparatus for optical measurement of bilirubin in tissue,” Jan. 17, 1992
- [129] J. A. Taylor *et al.*, “Use of a smartphone app to assess neonatal jaundice,” *Pediatrics*, vol. 140, no. 3, 2017, doi: 10.1542/peds.2017-0312.

- [130] A. M. Laughney *et al.*, “System analysis of spatial frequency domain imaging for quantitative mapping of surgically resected breast tissues,”
<https://doi.org/10.1117/1.JBO.18.3.036012>, vol. 18, no. 3, p. 036012, Mar. 2013,
doi: 10.1117/1.JBO.18.3.036012.
- [131] A. Mazhar, S. A. Sharif, J. David Cuccia, J. S. Nelson, K. M. Kelly, and A. J. Durkin, “Spatial Frequency Domain Imaging of Port Wine Stain Biochemical Composition in Response to Laser Therapy: A Pilot Study,” *Lasers in Surgery and Medicine*, vol. 44, pp. 611–621, 2012, doi: 10.1002/lsm.22067.
- [132] C. Romagnoli *et al.*, “BiliCheck vs JM-103 in identifying neonates not at risk of hyperbilirubinaemia,” *Italian Journal of Pediatrics*, vol. 39, no. 1, pp. 1–6, Jul. 2013, doi: 10.1186/1824-7288-39-46/FIGURES/1.
- [133] D. Jones *et al.*, “A Prospective Comparison of Transcutaneous and Serum Bilirubin Within Brief Time Intervals,” *Clinical Pediatrics*, vol. 56, no. 11, pp. 1013–1017, 2017, doi: 10.1177/0009922817701170.